ISSN 0915-633X

NATIONAL INSTITUTE FOR FUSION SCIENCE

RF Helicity Injection and Current Drive

K. Hamamatsu, A. Fukuyama, S.-I. Itoh, K. Itoh and M. Azumi

(Received – June 14, 1990)

NIFS-34 July 1990

RESEARCH REPORT
NIFS Series

NAGOYA, JAPAN

RF helicity injection and current drive

K. Hamamatsu

Department of Large Tokamak Research,
Naka Fusion Research Establishment,
Japan Atomic Energy Research Institute,
Naka, Ibaraki 311-01, JAPAN

A. Fukuyama

Faculty of Engineering,
Okayama University,
Okayama 700, JAPAN

S.-I. Itoh, K. Itoh

National Institute for Fusion Science,
Chikusa, Nagoya 464-01, JAPAN

M. Azumi

Department of Large Tokamak Research,
Naka Fusion Research Establishment,
Japan Atomic Energy Research Institute,
Naka, Ibaraki 311-01, JAPAN

ABSTRACT

The relation between RF-driven current and wave helicity is analytically and numerically studied for a tokamak plasma. The helicity conversion coefficient from the wave to the plasma is generally obtained and numerically examined for the waves in the range of ion cyclotron frequency. The wave propagation equation which includes kinetic effects is solved as a boundary-value problem with one-dimensional inhomogeneities. It is shown that the wave helicity well satisfies the continuity equation. We confirm that the RF-helicity injection is not an identical phenomenon of the reduction of the one turn loop voltage due to the RF-driven current.

Keywords; RF helicity, ICRF wave, Helicity injection, Current drive

I. INTRODUCTION

For stationary operation of a tokamak-type fusion reactor, the development of an efficient current drive scheme in a high-density plasma is one of the issues with highest priority. The current drive experiments using the lower-hybrid wave and the neutral beam injection have demonstrated high current-drive efficiency in a low density regime. The efficiency of such current drive schemes, which employ the injection of the momentum or the sustainment of an anisotropic velocity distribution, is inversely proportional to the plasma density and the current sustainment in a reactor-relevant plasma requires very large input power.[1-7]

As an alternative non-ohmic current drive scheme, the method based on magnetic helicity injection has also attracted a lot of attentions.[8-14] The helicity injection on a magnetohydrodynamic time scale, such as the F-Θ pumping and the peripheral beam injection, has been studied both theoretically and experimentally.[15-22]

The injection by RF-waves with helicity has been proposed[23,24] as a promising current drive scheme and the current-drive efficiency is reportedly independent of the plasma density.[24] Recently, the relation between RF-driven current and helicity conservation is clearly explained in Refs.25 and 26 . Since the previous calculations are local analyses, however, the problem remains whether the current is actually driven by the stationary-excited wave in a realistic geometry. The amount of the helicity-driven current resulted from the $\tilde{\mathbf{v}} \times \tilde{\mathbf{B}}$ force should be calculated by solving the global wave structure self-consistently. Furthermore, it has not been clarified how much the helicity injected by the transversely-polarized wave is converted to the DC helicity associated with the plasma current. And the relation between the conventional current drive by the momentum injection and the newly-proposed one by the RF-helicity injection should be identified.

In the present paper, the RF-oscillating time is much shorter than the plasma relaxation time. The typical phenomena of the relaxation process such as the magnetic

reconnection does not occur in the RF-oscillating time. From this view point, we derive the conservation law of the helicity associated with the stationary RF-wave and examine the contribution to the current drive. The relation between the momentum absorption and the helicity absorption is also discussed. After the general formulation, we concentrate on the behavior of wave in the ion cyclotron range of frequencies(ICRF). We solve the wave propagation as a boundary value problem in a slab geometry[27] and calculate the profile of the electron current including the contribution from the $\tilde{\mathbf{v}} \times \tilde{\mathbf{B}}$ force. The density dependence of the current drive efficiency is obtained. In addition to the electron current, the ion current driven near the ion cyclotron resonance is also examined. In the presence of fast ions injected by a neutral beam, we estimate the incremental current-drive efficiency due to the ICRF waves.

In §2, we present the general properties of the helicity associated with the RF wave and discuss its relation with the current drive. The specific calculation of the current drive using the ICRF wave with helicity is described in §3. Following the description of the model used in the calculation, the results of the global analysis of the ICRF current drive are given. Both the electron current in the frequency away from the ion cyclotron resonance and the ion current near the ion cyclotron resonance are examined. The effect of a fast ion tail is also described. The summary and discussions are given in the §4.

II. RF-HELICITY AND CURRENT-DRIVE

We introduce the vector potential $\mathbf{A}$ ($\nabla \times \mathbf{A} = \mathbf{B}$) and write $\mathbf{A} = \mathbf{A}_0 + \tilde{\mathbf{A}}$, where the suffix '0' stands for the stationary component sustained by the Ohmic drive and the symbol '$\tilde{a}$' denotes the RF oscillation components. The helicity density $\mathcal{H}$ is defined as $\mathcal{H} = <\mathbf{A} \cdot \mathbf{B}>$ and can be written as

$$\mathcal{H} = \mathcal{H}_{\rm OH} + \mathcal{H}_{\rm RF}, \tag{1}$$

and

$$\mathcal{H}_{\rm RF} = <\tilde{\mathbf{A}} \cdot \tilde{\mathbf{B}}> . \tag{2}$$

Here <> indicates the time average over the wave period, i.e., $<\mathbf{a}\cdot\mathbf{b}>=(\mathbf{a}^*\cdot\mathbf{b}+\mathbf{a}\cdot\mathbf{b}^*)/2$, where the symbol '$*$' denotes the complex conjugate. . In order to drive the dc electric field, $\mathbf{E}_{\mathrm{OH}}$, the vector potential $\mathbf{A}_0$ changes slowly. The time scale of the change is the resistive diffusion time and is much slower than the RF frequency ω. In treating the time average <>, we approximate that $\mathbf{A}_0$ is constant over the wave period. Noting the relations $\tilde{\mathbf{E}}=-\nabla\tilde{\phi}-\partial\tilde{\mathbf{A}}/\partial t$ and $\tilde{\mathbf{B}}=\nabla\times\tilde{\mathbf{A}}$, the conservation of the RF helicity density is written as

$$\frac{\partial}{\partial t}(\tilde{\mathbf{A}}\cdot\tilde{\mathbf{B}})+\nabla\cdot\left(\tilde{\mathbf{A}}\times\frac{\partial\tilde{\mathbf{A}}}{\partial t}+2\tilde{\phi}\tilde{\mathbf{B}}\right)=-2\tilde{\mathbf{E}}\cdot\tilde{\mathbf{B}}, \tag{3}$$

Taking the time average and summing up the OH component, we have

$$\frac{\partial\mathcal{H}}{\partial t}+\nabla\cdot\left(\mathbf{A}_0\times\frac{\partial\mathbf{A}_0}{\partial t}\right)+\nabla\cdot\left(\left\langle\tilde{\mathbf{A}}\times\frac{\partial\tilde{\mathbf{A}}}{\partial t}\right\rangle+2\left\langle\tilde{\phi}\tilde{\mathbf{B}}\right\rangle\right)=-2\left\{\mathbf{E}_{\mathrm{OH}}\cdot\mathbf{B}_0+<\tilde{\mathbf{E}}\cdot\tilde{\mathbf{B}}>\right\},$$

$$\left\langle\tilde{\mathbf{A}}\times\frac{\partial\tilde{\mathbf{A}}}{\partial t}\right\rangle=\frac{1}{2}\Re\left(\tilde{\mathbf{A}}^*\times\frac{\partial\tilde{\mathbf{A}}}{\partial t}+\tilde{\mathbf{A}}\times\frac{\partial\tilde{\mathbf{A}}^*}{\partial t}\right), \tag{4}$$

where $\mathbf{B}_0$ is the external magnetic field, i.e., the toroidal magnetic field. In deriving Eq.(4), we note that operators ∇ and <> are commutable. If one defines the helicity fluxes $\mathbf{Q}_{\mathrm{OH}}$ and $\mathbf{Q}_{\mathrm{RF}}$ as

$$\mathbf{Q}_{\mathrm{OH}}=\mathbf{A}_0\times\frac{\partial\mathbf{A}_0}{\partial t}, \tag{5-1}$$

$$\mathbf{Q}_{\mathrm{RF}}=\left\langle\tilde{\mathbf{A}}\times\frac{\partial\tilde{\mathbf{A}}}{\partial t}\right\rangle+2<\tilde{\phi}\tilde{\mathbf{B}}>, \tag{5-2}$$

we have

$$\frac{\partial\mathcal{H}}{\partial t}+\nabla\cdot\mathbf{Q}_{\mathrm{OH}}+\nabla\cdot\mathbf{Q}_{\mathrm{RF}}=-2\mathbf{E}_{\mathrm{OH}}\cdot\mathbf{B}_0-2<\tilde{\mathbf{E}}\cdot\tilde{\mathbf{B}}>, \tag{6}$$

The right hand side is the helicity sink/source term. Equations (3) to (5) form the conservation relation of helicity. It is noted that the OH part and RF part satisfy the conservation relations

$$\nabla\cdot\mathbf{Q}_{\mathrm{OH}}=-2\mathbf{E}_{\mathrm{OH}}\cdot\mathbf{B}_0, \tag{7-1}$$

$$\nabla\cdot\mathbf{Q}_{\mathrm{RF}}=-2<\tilde{\mathbf{E}}\cdot\tilde{\mathbf{B}}>, \tag{7-2}$$

in the stationary state.

From Eq.(5-2), one sees that the RF helicity flux has two contributions. One is the $\left\langle \tilde{\mathbf{A}} \times \partial\tilde{\mathbf{A}}/\partial t \right\rangle$ term and the other is the $2\left\langle \tilde{\phi}\tilde{\mathbf{B}} \right\rangle$ term. The former term has contribution when the RF amplitude is growing (or decaying) in time or when the RF-wave has the circularly polarized component.[23-24] It disappears for plane waves in the stationary state where the relation $\partial\tilde{\mathbf{A}}/\partial t = -\mathrm{i}\omega\tilde{\mathbf{A}}$ holds. The current drive by RF helicity, which is associated with th temporal change of RF amplitude, has been discussed in literatures. Such contribution, however, vanishes in a stationary state, in which wave amplitude stays constant.

The balance between the divergence of the helicity flux and helicity sink/source is given by Eq.(6). The main problems are whether the injected RF helicity flux $\mathbf{Q}_{\mathbf{RF}}$ can save the OH helicity flux $\mathbf{Q}_{\mathbf{OH}}$ and how large the conversion coefficient between them is. To obtain the relation between $\nabla \cdot \mathbf{Q}_{\mathbf{RF}}$ and change of $\nabla \cdot \mathbf{Q}_{\mathbf{OH}}$, we first study the RF dispersion by using the fluid model. Kinetic effects are studied in the next section.

The equation of motion and the continuity equation of density are given as

$$m\left(\frac{\partial \mathbf{v}}{\partial t} + \mathbf{v}\cdot\nabla\mathbf{v}\right) = q\left(\mathbf{E} + \mathbf{v}\times\mathbf{B}\right) - m\nu\mathbf{v}, \tag{8}$$

$$\frac{\partial n}{\partial t} + \nabla\cdot(n\mathbf{v}) = 0, \tag{9}$$

where m and q are the particle mass and charge and n and $\mathbf{v}$ are the density and the velocity. The collision frequency ν is evaluated as $\nu_{\mathbf{RF}}$ for the motion of the RF-wave frequency and $\nu_{\|}$ for the DC motion, respectively. Expanding the density n and velocity $\mathbf{v}$ as $n = n_0 + \tilde{n}_1 + \tilde{n}_2 + \cdots$ and $\tilde{\mathbf{v}} = \tilde{\mathbf{v}}_1 + \tilde{\mathbf{v}}_2 + \cdots$, the resultant current density is given as

$$\tilde{\mathbf{j}} = qn_0\tilde{\mathbf{v}}_1 + q(n_0\tilde{\mathbf{v}}_2 + \tilde{n}_1\tilde{\mathbf{v}}_1) + \cdots. \tag{10}$$

Here the suffix j denotes the j-th order quantity of the RF amplitude. We have

$$<\tilde{\mathbf{v}}_2>_{\|} = \frac{1}{\nu_{\|}B_0}\left[\frac{q}{m} <\tilde{\mathbf{E}}_1\cdot\tilde{\mathbf{B}}_1> + \mathrm{i}(\omega + \mathrm{i}\nu_{\mathbf{RF}}) <\tilde{\mathbf{v}}_1\cdot\tilde{\mathbf{B}}_1> - <\tilde{\mathbf{v}}_1\cdot\nabla\tilde{\mathbf{v}}_1>\cdot\mathbf{B}_0\right]. \tag{11}$$

The RF driven current is given as

$$<\tilde{\mathbf{j}}_2>_{\parallel} = q\left(n_0 <\tilde{\mathbf{v}}_2>_{\parallel} + <\tilde{n}_1\tilde{\mathbf{v}}_1>_{\parallel}\right), \tag{12}$$

Using the relation $n_1 = -\mathrm{i}\, n_0 \nabla\cdot\tilde{\mathbf{v}}_1/\omega = n_0\mathbf{k}\cdot\tilde{\mathbf{v}}_1/\omega$, Eq.(12) reduces to

$$<\tilde{\mathbf{j}}_2>_{\parallel} = \frac{q^2 n_0}{\nu_{\parallel} m}\left[\frac{<\tilde{\mathbf{E}}_1\cdot\tilde{\mathbf{B}}_1>}{B_0} + \mathrm{i}\,\frac{\omega+\mathrm{i}\nu_{\mathrm{RF}}}{\Omega_0} <\tilde{\mathbf{v}}_1\cdot\tilde{\mathbf{B}}_1> + \frac{\omega+\mathrm{i}\nu_{\parallel}}{\omega+\mathrm{i}\nu_{\mathrm{RF}}}\frac{\mathbf{k}}{\omega}\cdot <\tilde{\mathbf{v}}_1\tilde{\mathbf{E}}_1>\cdot\frac{\mathbf{B}_0}{B_0}\right], \tag{13}$$

where Ω_0 is the cyclotron frequency, eB_0/m. Here the wave vector $\mathbf{k}$ is determined by the dispersion relation, which is described by the Maxwell equation with the RF induced current, $\tilde{\mathbf{j}}_1 = qn_0\tilde{\mathbf{v}}_1$. From this relation, we have

$$\eta_{\parallel} j_{\parallel} = E_{0\parallel} + \frac{<\tilde{\mathbf{E}}_1\cdot\tilde{\mathbf{B}}_1>}{B_0}\left[1 + \mathrm{i}\,\frac{\omega+\mathrm{i}\nu_{\mathrm{RF}}}{\Omega_0}\frac{<\tilde{\mathbf{v}}_1\cdot\tilde{\mathbf{B}}_1>}{<\tilde{\mathbf{E}}_1\cdot\tilde{\mathbf{B}}_1>}B_0 + \frac{\omega+\mathrm{i}\nu_{\parallel}}{\omega+\mathrm{i}\nu_{\mathrm{RF}}}\frac{\frac{\mathbf{k}}{\omega}\cdot <\tilde{\mathbf{v}}_1\tilde{\mathbf{E}}_1>\cdot\mathbf{B}_0}{<\tilde{\mathbf{E}}_1\cdot\tilde{\mathbf{B}}_1>}\right] \tag{14}$$

where $\eta_{\parallel}$ is the resistivity. Under the constraint that the parallel current is fixed, the right hand side of Eq.(14) is constant. We have the reduction of the OH electric field, $-\delta E_{0_{\parallel}}$, satisfies

$$-\left(\delta E_{0_{\parallel}} B\right) = \lambda <\tilde{\mathbf{E}}_1\cdot\tilde{\mathbf{B}}_1>, \tag{15}$$

where the coefficient λ is given as

$$\lambda = 1 + \mathrm{i}\,\frac{\omega+\mathrm{i}\nu_{\mathrm{RF}}}{\Omega_0}\frac{<\tilde{\mathbf{v}}_1\cdot\tilde{\mathbf{B}}_1>}{<\tilde{\mathbf{E}}_1\cdot\tilde{\mathbf{B}}_1>}B_0 + \frac{\omega+\mathrm{i}\nu_{\parallel}}{\omega+\mathrm{i}\nu_{\mathrm{RF}}}\frac{\frac{\mathbf{k}}{\omega}\cdot <\tilde{\mathbf{v}}_1\tilde{\mathbf{E}}_1>\cdot\mathbf{B}_0}{<\tilde{\mathbf{E}}_1\cdot\tilde{\mathbf{B}}_1>}, \tag{16}$$

Noting that the conservation relation $\nabla\cdot\mathbf{Q}_{\mathrm{OH}} = -2E_{\mathrm{OH}}B_0$ and $\nabla\cdot\mathbf{Q}_{\mathrm{RF}} = -2<\tilde{\mathbf{E}}\cdot\tilde{\mathbf{B}}>$ holds independently, we have the change of OH helicity injection in terms of RF helicity flux as

$$-\delta(\nabla\cdot\mathbf{Q}_{\mathrm{OH}}) = \lambda\,\nabla\cdot\mathbf{Q}_{\mathrm{RF}}. \tag{17}$$

From these relations, the coefficient λ may be interpreted as the conversion coefficient of the RF helicity to the OH helicity under the constraint of the constant current and the constant resistivity.

The conversion coefficient λ obtained here is not necessarily unity. This means that the evaluation of the current drive efficiency by the relation $\lambda = 1$, i.e., $\delta(\int \mathbf{Q}_{\mathrm{OH}} \cdot d\mathbf{S}) = \int \mathbf{Q}_{\mathrm{RF}} \cdot d\mathbf{S}$ is not appropriate. The coefficient λ is **not** constrained by the conservation of **total** helicity, but dictated by other mechanism of current drive.

The driving mechanism is more clearly shown. In Eq.(11), the third term in the right hand side $\mathbf{v} \cdot \nabla \mathbf{v}$ comes from the centrifugal force and the compressibility ($\tilde{E}_{\parallel}$ contribution). The first and second terms are due to the $\tilde{\mathbf{v}} \times \tilde{\mathbf{B}}$ force, which is usually accounted for in evaluating dynamo force. From Eq.(8), the $<\tilde{\mathbf{v}} \times \tilde{\mathbf{B}}>$-driven current satisfies

$$\eta_{\parallel} j_{\parallel}^{\tilde{\mathbf{v}}\times\tilde{\mathbf{B}}} = \frac{q}{m}\left\{ \mathrm{i}\frac{\omega + \mathrm{i}\nu_{\mathrm{RF}}}{\Omega^2 - (\omega + \mathrm{i}\nu_{\mathrm{RF}})^2}\left\langle (\tilde{\mathbf{E}} \times \tilde{\mathbf{B}})_{\parallel} \right\rangle + \frac{\Omega}{\Omega^2 - (\omega + \mathrm{i}\nu_{\mathrm{RF}})^2}\left\langle \tilde{\mathbf{E}}_{\perp} \cdot \tilde{\mathbf{B}}_{\perp} \right\rangle \right\}. \tag{18}$$

The first term is the damping of the wave due to the polarization drift and the second term is that due to the $<\tilde{\mathbf{E}}_1 \times \mathbf{B}_0>$ drift motion. If the RF wave approaches to the single plane wave, i.e., $\tilde{\mathbf{B}}_1$ approaches to $\mathbf{k} \times \tilde{\mathbf{E}}/\omega$, the $<\tilde{\mathbf{E}} \cdot \tilde{\mathbf{B}}>$ term disappears and the driven current comes from $<\tilde{\mathbf{E}} \times \tilde{\mathbf{B}}>$ term. This term is proportional to the damping of the parallel Poynting flux. In such a case, λ can be very large number: This large value of λ does not mean that the current-drive efficiency is high. Equation(18) shows that the phase-relation of the wave is the key parameter for the conversion coefficient.

III. NUMERICAL RESULTS IN THE ION CYCLOTRON RANGE OF FREQUENCY

In this section we present the numerical results obtained for the current drive due to the ICRF waves in a tokamak plasma. The relation between the driven current and RF-helicity is shown quantitatively. In the previous section, the relation was discussed using the fluid model in which the collisional absorption was the mechanism of dissipation, i.e., the collision frequency ν_{RF} was introduced as the typical wave-particle interaction frequency. And we did not restrict the wave structure and excitation spectrum.

The quantitative analysis, however, requires consistent description of excitation by an antenna, propagation in an inhomogeneous and dispersive medium and absorption through microscopic kinetic processes, such as Landau damping and cyclotron damping. There are two important kinetic effects on wave propagation. One is the wave-particle interaction which causes collisionless damping and spatial dispersion in the direction of static magnetic field. The other is the finite gyroradius effect which results in the dispersion perpendicular to the magnetic field. Furthermore, these effects are determined by the analysis of global wave structure. In order to calculate the RF wave driven current and RF helicity, we include these kinetic effects and obtain exactly the spatial profile of RF wave amplitude $(\tilde{\mathbf{A}}, \tilde{\phi})$. For the ICRF waves, the modeling and numerical procedure of the global waves in one dimensional geometry has been developed by Fukuyama et.al.[27] Using this numerical analysis code, we analyze the global structure of the RF driven current and RF helicity.

This section is divided by three parts as follows. In subsection 3-A, the model of the ICRF wave propagation is explained. The numerical results of the electron driven current and ion driven current are shown in 3-B and 3-C, respectively.

A. KINETIC MODEL OF WAVE PROPAGATION AND CURRENT DRIVE

To obtain the RF-driven current, it is necessary to calculate the velocity distribution function in the existence of the wave excitation. The form of the lowest-order turbulent velocity diffusion, is investigated in the quasi-linear theory by Kennel and Engelmann,[28] where two components of RF-driven force, $\tilde{\mathbf{v}} \times \tilde{\mathbf{B}}$ and $\tilde{\mathbf{v}} \cdot \nabla \tilde{\mathbf{v}}$ terms, are taken into account. We estimate the RF-driven current from the balance between the RF-driven force and collision force. The wave fields in the plasma are calculated taking account of the wave excitation by antenna, propagation and absorption in an inhomogeneous plasma.

Quasi-linear theory separates the velocity distribution function $f_s(\mathbf{r}, \mathbf{v}, t)$ into slowly varying component $f_{s0}(\mathbf{v}, \mathbf{r}, t)$ and small, rapidly fluctuating part $\tilde{f}_s(\mathbf{r}, \mathbf{v}, t)$ due

to waves, where the suffix s denotes the particle species. We can divide the Vlasov equation into two parts:

$$\frac{\partial \tilde{f}_s}{\partial t} + \mathbf{v} \cdot \frac{\partial \tilde{f}_s}{\partial \mathbf{r}} + \frac{q_s}{m_s}(\tilde{\mathbf{E}} + \mathbf{v} \times \tilde{\mathbf{B}}) \cdot \frac{\partial f_{s0}}{\partial \mathbf{v}} = 0, \tag{19}$$

$$\frac{\partial f_{s0}}{\partial t} + \mathbf{v} \cdot \frac{\partial f_{s0}}{\partial \mathbf{r}} + \frac{q_s}{m_s}(\mathbf{v} \times \mathbf{B}_0) \cdot \frac{\partial f_{s0}}{\partial \mathbf{v}} + \frac{q_s}{m_s} \left\langle (\tilde{\mathbf{E}} + \mathbf{v} \times \tilde{\mathbf{B}}) \cdot \frac{\partial \tilde{f}_s}{\partial \mathbf{v}} \right\rangle = 0, \tag{20}$$

Equation (19) determines the fluctuated velocity distribution function of the plasma. The RF-fields, $\tilde{\mathbf{E}}$ and $\tilde{\mathbf{B}}$, are determined by the Maxwell equation with the RF-induced current, which is obtained by $\tilde{f}_s$. The time-development of f_{s0} component is described by Eq.(20).

The wave equation is obtained from the Maxwell equation as follows:

$$\nabla \times \nabla \times \tilde{\mathbf{E}} + \frac{\omega^2}{c^2}\tilde{\mathbf{E}} = \mathrm{i}\, \mu_0 \omega (\sum_s \tilde{\mathbf{j}}_s + \tilde{\mathbf{j}}_A), \tag{21}$$

where $\tilde{\mathbf{j}}_s$ is the oscillating current carried by the s-th species and $\tilde{\mathbf{j}}_A$ is the antenna oscillating current with the frequency ω. The RF-oscillating current $\tilde{\mathbf{j}}_s$ is calculated by $\int d\mathbf{v} q_s \mathbf{v} \tilde{f}_s$. This is reduced to the conventional form using the non-local kinetic conductive tensor; $\tilde{\mathbf{j}}_s = \int d\mathbf{r}' \sigma(\mathbf{r} - \mathbf{r}', \omega, \mathbf{r} + \mathbf{r}') \cdot \tilde{\mathbf{E}}(\mathbf{r}')$. We assume that the plasma is in the steady state and the deviation of f_{s0} from the Maxwellian distribution is very small. The explicit form of $\tilde{\mathbf{j}}_s$ is given in Ref. 27, where the f_{s0} is treated as the Maxwellian. The Landau damping(LD), transit time magnetic pumping (TTMP) and the cyclotron damping near the fundamental and second harmonic resonances are included.

The wave equation, Eq.(21), is solved in the one dimensional slab geometry, where the straight magnetic field aligns along the z-direction (toroidal-direction) and its magnitude varies in the x-direction (direction of minor radius). The toroidal magnetic field also varies in the x-direction as $B_0(x) = B_0(0)/(1 + x/R)$. The antenna current $\tilde{\mathbf{j}}_A$ carries the sheet current along the y-direction (poloidal direction). The plasma parameters, i.e., density and temperature are assumed to vary in the x-direction and to be

homogeneous in the y and z-directions:

$$n_s(x) = [n_s(0) - n_s(a)]\left[1 - \left(\frac{x}{a}\right)^2\right] + n_s(a),$$
$$T_s(x) = T_s(0)\exp\left[-3\left(\frac{x}{a}\right)^2\right]. \tag{22}$$

The periodic boundary condition is employed in the z-direction and the wave equation is Fourier-decomposed (k_z) in this direction. Under the above assumptions, the differential wave equation with respect to x is solved with the boundary condition on the wall and exciting condition at the antenna.

The numerical procedure for solving the wave equation is as follows: The inhomogeneous plasma is divided into thin uniform layers and the local dispersion relation is solved in each layer. There are six independent solutions in each layer and the electric field is expressed by a linear combination of these modes, i.e.,

$$\tilde{\mathbf{E}}(x) = \sum_{l=1}^{6} C_l \mathbf{P}_l \exp[\mathrm{i}\,(k_{lx}x + k_{lz}z - \omega t)], \tag{23}$$

where the polarization vector $\mathbf{P}_l$ is obtained by the local dispersion relation. The arbitrary constant C_l is determined so that all the continuity conditions on the interfaces between the uniform plasma layers and on the plasma/vacuum interfaces are satisfied. It is important that the electric field is described by the combination of six eigen modes. If we take only a single mode, the helicity sink/source term $<\tilde{\mathbf{E}}\cdot\tilde{\mathbf{B}}>$ disappears .

The RF-driven static force is obtained from the velocity moment in the z-direction of Eq.(20). Because the plasma is assumed to be stationary, we estimate the drift velocity by balancing the RF-force with the collisional drag. We have

$$\nu_{\parallel} < \mathbf{v}_s >_{\parallel} = \frac{1}{m_s n_s}\left\langle \tilde{E}_z\tilde{\rho}_s + (\tilde{\mathbf{j}}_s \times \tilde{\mathbf{B}})_z \right\rangle, \tag{24}$$

where $\tilde{\rho}_s$ is the space charge density. In this expression, we neglect the pressure driven force which is originated from the second term in Eq.(20). Using the relations, $\tilde{\rho}_s = (\mathbf{k}\cdot\tilde{\mathbf{j}}_s)/\omega$ and $\tilde{\mathbf{B}} = (\mathbf{k}\times\tilde{\mathbf{E}})/\omega$, the RF-driven current is obtained as

$$j_{\parallel s}(x) = \frac{q_s}{m_s\nu_{\parallel}}\frac{k_z}{\omega}P_s(x). \tag{25}$$

Here $P_s(x) = \left\langle \tilde{\mathbf{E}}(x) \cdot \tilde{\mathbf{j}}_s(x) \right\rangle$ is an absorbed wave energy by the s-th species particles. Equation(25) means that the RF-current drive is caused by the momentum transfer. Therefore, we notice that ion driven current and electron driven current have opposite sign.

In the following subsections, we present numerical results. We use typical parameters of JT-60 plasma as standard ones: $R = 3\text{m}$, $B_0(0) = 4\text{T}$, $a = 0.95\text{m}$, $T_e(0) = T_i(0) = 10\text{keV}$, $n_e(0) = 3 \times 10^{20}\text{m}^{-3}$, and $n_e(a) = 0.1 \times n_e(0)$, $Z_{\text{eff}} = 2.4$. In order to reproduce the experimentally-observed Z_{eff}, 2.4, we include the oxygen impurity ion the concentration of which is 2.5 % of the electron density.

B. ELECTRON DRIVEN CURRENT

The numerical results for the electron driven current is presented in this section. To avoid the ion cyclotron resonance, we choose the low frequency, $f = 40\text{MHz}$ ($\omega < \Omega_0$). Figure 1 shows the electric field pattern (E_y), power deposition profile and driven current profile, respectively. In this calculation, the parallel wave vector is fixed at $k_z = 9\,\text{m}^{-1}$ and the antenna sheet current is 1 A/m. The x-axis indicates the distance from the plasma axis on the midplane. The fast wave is launched from the low-field side ($x > 0$). Although the proton cyclotron resonance is away from the low-field side, the cyclotron resonance of the heavy impurity, the oxygen ion, locates $x \sim -0.7\,\text{m}$ and the fast wave is reflected at the two-ion hybrid cutoff layer, $x \sim -0.25\,\text{m}$. Since the damping of the fast wave is very weak, a standing wave is excited between the cutoff layer and the low-field-side wall. The corrugated power deposition profile corresponds to the nodes and loops of the electric field. The wave energy is mainly absorbed by electrons owing to TTMP and LD in the absence of the ion cyclotron resonance. Because the RF-driven current is proportional to the absorbed wave energy, the radial profile of driven current has a similar structure with corrugation.

Figure 2 shows the spatial profiles of the RF-helicity flux Q_{RF} (Eq.(5-2)), the helicity sink/source term $< \tilde{\mathbf{E}} \cdot \tilde{\mathbf{B}} >$ and the reduction of the OH electric field $\delta E_{\parallel} B_0$ (Eq.(15)), where we choose the Coulomb gauge. The RF helicity conservation relation

(7-2) is well satisfied. In the estimation of OH electric field, we use the formula of plasma resistivity

$$\eta_{\parallel} = Z_{\rm eff}\frac{m_e^{1/2}e^2\ln\Lambda}{6\pi\sqrt{2\pi}\epsilon_0^2 T_e^{3/2}} \quad \text{and} \quad Z_{\rm eff} = \frac{\sum_{\rm i} Z_{\rm i}^2 n_{\rm i}}{\sum_{\rm i} Z_{\rm i} n_{\rm i}} \tag{26}$$

and constant current condition is employed. We see that the spacial profiles of the quantities $<\tilde{\mathbf{E}}\cdot\tilde{\mathbf{B}}>$ and $\delta E_{\parallel}B_0$ are quite different. We confirm the fact that the RF-helicity injection is not an identical phenomenon to the reduction of the one turn loop voltage.

Figure 3 shows the k_z-dependences of global quantities. The dependence of total absorbed power $\bar{P}_s(=\int_{-a}^{a}dxP_s(x))$ is presented in Fig. 3(a). Electrons always absorb the main part of the wave energy in this case. The dashed curve, $\bar{P}_{\rm wall}$ shows the loss energy on the resistive wall, which is negligibly small. Figures 3(b) and 3(c) show the global driven current (b) and the drive efficiency (c), which is defined by

$$\bar{\eta}_{\rm CD} = \frac{\bar{n}_e R\int_{-a}^{a}dx\sum_s j_{\parallel s}(x)}{\sum_s \bar{P}_s}, \tag{27}$$

respectively. The current drive efficiency increases linearly with increase of k_z. Since the conductivity is proportional to $T_e^{3/2}/n_e$ and the spatial profile is given by Eq.(22), the conductivity decreases near the plasma surface and the current drive efficiency also decreases. The global conversion efficiency of the wave helicity, $\bar{\lambda}$, may be defined as

$$\bar{\lambda} = -\frac{\int_{-a}^{a}dx\delta E_{\rm OH}B(x)}{\int_{-a}^{a}dx\left\langle\tilde{\mathbf{E}}_1(x)\cdot\tilde{\mathbf{B}}_1(x)\right\rangle} = 2\frac{\int_{-a}^{a}dx\delta E_{\rm OH}B(x)}{Q_{\rm RFx}(a)-Q_{\rm RFx}(-a)} \tag{28}$$

from Eq.(15). In Fig. 3(d) we show k_z dependence of $\bar{\lambda}$. The absolute value of $\bar{\lambda}$ has a maximum value about 500 near $k_z = 3\,{\rm m}^{-1}$ and decreases with the increase of k_z. Since $|\bar{\lambda}|$ is much greater than unity, most of the current is driven by the momentum transfer which does not accompany with the helicity transfer. We see that the highest

efficiency of the wave helicity conversion does not correspond to the highest current-drive efficiency.

C. ESTIMATION OF ION CURRENT

The absorption of wave helicity takes place in a case where waves are absorbed by ions through cyclotron damping.[24] We estimate the driven current in the case of ion cyclotron resonance. The $<\tilde{\mathbf{v}} \times \tilde{\mathbf{B}}>$ force also appears for ions. The ion flow driven by the $<\tilde{\mathbf{v}} \times \tilde{\mathbf{B}}>$ force is estimated. The Ohkawa current[5] associated with this ion flow is evaluated by using the neoclassical formula.[29]

The drift velocity of resonating ions are given as

$$v_{\mathrm{d}_\parallel} = \frac{1}{\nu_s m_\mathrm{i} n_\mathrm{i}} \left[< \tilde{E}_z \tilde{\rho}_\mathrm{i} > + < \tilde{\mathbf{j}}_\mathrm{i} \times \tilde{\mathbf{B}} >_\parallel \right] \tag{29}$$

where ν_s^{-1} is the slowing down time of ions. The net current $j_{\mathrm{i}\,\parallel}$ is given as

$$j_{\parallel \mathrm{i}} = h(v_{\mathrm{d}_\parallel}) q_\mathrm{i} n_\mathrm{i} v_{\mathrm{d}_\parallel} \tag{30}$$

where the coefficient $h(v_{\mathrm{d}_\parallel})$, which represents the effects of electron shielding and trapped particles, is given in Ref. 29.

Figure 4 illustrates the case of second cyclotron resonance heating: Power partition (a), driven current (b), current driven efficiency (c) and helicity conversion coefficient (d). The wave frequency is 120 MHz and other parameters are the same as in Fig. 3. The ion absorption is stronger for longer wave length modes ($k_z \leq 12\,\mathrm{m}^{-1}$) and comparable to electrons for shorter wave length modes. The current carried by electrons are originated from absorption through TTMP and LD. The absorption of the longer wave length modes by ions gives only a small amount of the driven current. Due to the strong ion absorption, the total current drive efficiency is lower than the cases in the previous subsection.

The ion driven current can be large if there exist fast ions and the wave is absorbed by the fast ions. We here examine the RF-assist of the beam induced current. We assume that the plasma ion has two components. The hot component represents, for instance,

fast ions produced by the neutral beam injection. If the RF waves are absorbed by the fast ions ($v \gg v_{\rm thi}$), the slowing-down time is estimated by $\nu_{\rm ie}$. In such a situation, the incremental current by the RF-induced force is given by

$$j_{\parallel \rm i} = h(v_{\rm b\parallel}) \frac{q_{\rm i}}{m_{\rm i}\,\nu_{\rm ie}} \left[< \tilde{E}_z \tilde{\rho}_{\rm b} > + < \tilde{\mathbf{j}}_{\rm b} \times \tilde{\mathbf{B}} >_{\parallel} \right], \tag{31}$$

where $v_{\rm b}$ is the typical beam velocity and $\tilde{\mathbf{j}}_{\rm b}$ is the RF-oscillating current carried by beam ions. Due to long slowing-down time, the induced current is much enhanced.

Figure 5 shows the case of second cyclotron resonance heating in the presence of hot ions. The concentration of the tail ion $n_{\rm b}$ is 8 % of $n_{\rm e}$ and the tail temperature is 300 keV. Other parameters are the same as Fig. 3. The fast ions absorb most of the power. Figure 5(b) shows that the RF-driven ion current which flows in the opposite direction to the electron current has the largest contribution. The global conversion coefficient $\bar{\lambda}$ becomes positive. The current drive efficiency has a magnitude comparable with that in the case of electron current drive.

Figure 6 illustrates the spatial profiles of $P_{\rm abs}$, $j_{\parallel \rm i}$, $Q_{\rm RF}$, $<\tilde{\mathbf{E}} \cdot \tilde{\mathbf{B}}>$ and $\delta E_{\parallel} B_0$ in the case of $k_z = 20\,{\rm m}^{-1}$. The current is driven in the region $r \sim a/2$ where the beam ions absorb the wave through the Doppler-shifted second-harmonic cyclotron resonance. The helicity dissipation rate becomes negative and the helicity flux increases within a plasma. This phenomena suggests the possibility of the modification of the current profile due to the helicity transport.

The density dependence of the current drive efficiency is shown in Fig. 7. The efficiency is calculated for various values of $n_{\rm e0}$ and $T_{\rm bulk}$ keeping $n_{\rm b}/n_{\rm e} = 0.08$. The wave number k_z is so chosen that the efficiency is maximized for given plasma parameters. When the temperature of the beam $T_{\rm b}$ is low (100 keV), the ion current slightly exceeds the electron current which flows in the opposite direction. There is a lower bound of hot ion temperature to obtain a high current drive efficiency. The efficiency is approximately proportional to $T_{\rm b}$ for $T_{\rm b} > 100\,{\rm keV}$. In this region, $\bar{\eta}_{\rm CD}$ has weak positive dependence on $n_{\rm e0}$.

IV. SUMMARY AND DISCUSSIONS

We have studied the relation between the RF helicity injection and the RF current drive. The formula of the RF helicity in a stationary state has been derived for the RF waves, whose frequency is much higher than that of the conventional helicity injection. The helicity density, helicity density flux and dissipation rate have been introduced and the relation of the injected RF helicity to the DC helicity has been clarified. The efficiency of RF current drive has been examined and the helicity conversion factor from the wave to the plasma has been obtained. It is found that the RF helicity injection is not an identical phenomenon of the reduction of the one turn loop voltage. It may cause a misleading result if one counts the current drive efficiency, $\eta_{\rm CD}$, from helicity balance equation.

The helicity conversion in the MHD analysis is attributed to the turbulent relaxation. In a turbulent state, the phase between $\tilde{\mathbf{v}}$ and $\tilde{\mathbf{B}}$ is assumed to be random and the net force remains. On the other hand, the phase difference is determined from the wave propagation in the analysis of the RF helicity injection. The force is consistently obtained by solving the wave propagation equation and the induced helicity is estimated.

Application study has been made for ICRF waves. The wave propagation has been solved to obtain the phase relation of the electromagnetic field. The spatial profile of the RF helicity flux as well as the helicity dissipation has been calculated. The current drive efficiency, $\eta_{\rm CD}$, has been estimated and its k_z dependence as well as the dependence on the plasma density have been obtained. The helicity conversion factor, $\bar{\lambda}$, is much higher than unity for the parameter range in the present calculation. Most of the current is driven by the momentum transfer from the wave to the electrons through TTMP.

The smallness of the RF driven current associated with the helicity injection would be attributed to the low electron temperature. The local analysis[26] has shown strong

temperature dependence of the current drive efficiency through the helicity injection. The performance in a reactor-grade plasma will be examined in our forthcoming paper.

With respect to the ion current, the contribution of the thermal ion component has been found to be small. The direction of the current is opposite to the electron current. If the high-energy tail component presides owing to NBI, for example, the induced ion current becomes large. The density dependence of the efficiency is weaker than $1/n$. We found that the helicity dissipation rate can be negative, *i.e.*, the helicity can be generated within a plasma. This phenomena suggests the possibility of the modification of the current profile.

In order to obtain more quantitative results, the Fokker-Planck analyses are necessary for both electron and ion components. In particular, the existence of trapped particles changes the efficiency and further careful analysis is needed.

ACKNOWLEDGEMENTS

Authors would like to thanks Dr. Ohkawa for elucidating (and creative) discussions. Thanks are also due to Drs. S. Tamura, M. Yoshikawa, Y. Furutani and A. Iiyoshi for encouragement. The work has been done under the collaboration between JAERI-Universities on fusion research. The work is also partly supported by Grant-in-Aid for Fusion Research and the Grant-in-Aid for Scientific Research of the Ministry of Education in Japan.

REFERENCES

[1] N. J. Fisch, Rev. Mod. Phys. **59**, 175 (1987).

[2] N. J. Fisch, Nucl. Fusion **21**, 15 (1981).

[3] N. J. Fisch and A. H. Boozer, Phys. Rev. Lett. **45**, 720 (1980).

[4] A. H. Boozer, Phys. Fluids **31**, 591 (1988).

[5] T. Ohkawa, Nucl. Fusion **10**, 185 (1970).

[6] J. G. Cordey, Plasma Phys. **26**, 123 (1984).

[7] Y. Kishimoto, K. Hamamatsu, A. Fukuyama, S.-I. Itoh and K. Itoh, Nucl. Fusion **27**, 549 (1987).

[8] J. M. Finn and T. M. Antonsen, Comments on Plasma Physics and Controlled Fusion **9**, 111 (1985).

[9] A. Pouquet and G. S. Patterson, J. Fluid Mech. **85**, 305 (1978).

[10] M. A. Berger and G. B. Field, J. Fluid Mech. **147**, 133 (1984).

[11] J. B. Taylor, Phys. Rev. Lett. **33**, 1139 (1974).

[12] J. B. Taylor, Rev. Mod. Phys. **58**, 741 (1986).

[13] A. Reiman, Phys. Fluids **24**, 956 (1981).

[14] A. H. Boozer, Phys. Fluids **29**, 4123 (1986).

[15] T. H. Jensen and M. S. Chu, Phys. Fluids **27**, 2881 (1984).

[16] P. M. Bellan, Phys. Fluids **27**, 2191 (1984).

[17] P. M. Bellan, Phys. Rev. Lett. **54**, 1381 (1985).

[18] P. M. Bellan, Nucl. Fusion **29**, 78 (1989).

[19] J. M. Finn, Phys. Fluids **29**, 2630 (1986).

[20] K. F. Schoenberg, C. J. Buchenauer, R. S. Massey, J. G. Melton, R. W. Moses, R. A. Nebel and J. A. Phillips, Phys. Fluids **27**, 548 (1984).

[21] J. B. Taylor and M. F. Turner, Nucl. Fusion **29**, 219 (1989).

[22] M. Ono, G. J. Greene, D. Darrow, C. Forest, H. Park and T. H. Stix, Phys. Rev. Lett. **59**, 2165 (1987).

[23] D. K. Bhadra and C. Chu, J. Plasma Phys. **33**, 257 (1985).

[24] T. Ohkawa, Comments on Plasma Physics and Controlled Fusion **12**, 165 (1989).

[25] R. R. Mett and J. A. Tataronis, Phys. Rev. Lett. **63**, 1380 (1989); J. B. Taylor, Phys. Rev. Lett. **63**, 1384 (1989).

[26] V. S. Chan, R. L. Miller and T. Ohkawa, Phys. Fluids, **B2**, 944 (1990); General Atomics Report GA-A19732, submitted to Phys.Fluids B.

[27] A. Fukuyama, S. Nishiyama, K. Itoh, S.-I. Itoh, Nucl. Fusion **23**, 1005 (1983).

[28] C. F. Kennel and F. Engelmann, Phys. Fluids **9**, 2377 (1966).

[29] S. P. Hirshman, Phys. Fluids **23**, 1238 (1980).

FIGURE CAPTIONS

Fig. 1 : The spatial profiles of (a) the wave electric field, (b) the absorbed power density, and (c) the driven current density. The wave frequency is 40 MHz, $k_z = 9\,\mathrm{m}^{-1}$ and other parameters are standard. In (a), the solid line, dashed-dotted line, and dotted line represent the absolute value, real part and imaginary part of the electric field E_y, respectively. The antenna location is indicated by a vertical dashed line.

Fig. 2 : The spatial profile of (a) the helicity flux, (b) the helicity dissipation rate, and (c) the reduction of the OH electric field. Parameters are the same as in Fig. 1.

Fig. 3 : The wave number dependence of (a) the absorbed power, (b) the driven current, (c) the current drive efficiency, and (d) the helicity conversion factor. The wave frequency is 40 MHz and other parameters are standard. The electron current drive due to momentum transfer through TTMP is dominant.

Fig. 4 : The wave number dependence of (a) the absorbed power, (b) the driven current, (c) the current drive efficiency, and (d) the helicity conversion efficiency. The wave frequency is 120 MHz and other parameters are standard. The second-harmonic ion cyclotron resonance absorbs the wave energy before it drives the electron current.

Fig. 5 : The wave number dependence of (a) the absorbed power, (b) the driven current, (c) the current drive efficiency, and (d) the helicity conversion factor. The beam component of ion, $n_\mathrm{b} = 0.08 n_\mathrm{e}$ and $T_\mathrm{b} = 300\,\mathrm{keV}$, is included. Other parameters are the same as in Fig. 4. The beam ions couple with the wave at the second-harmonic ion cyclotron resonance and the ion current is driven in the opposite direction to the electron current.

Fig. 6 : The spatial profiles of (a) the absorbed power density, (b) the driven current density, (c) the helicity flux, (d) the helicity dissipation rate, and (e) the reduction of the OH electric field. Parameters are the same as in Fig. 5.

Fig. 7 : The density dependence of the global current drive efficiency in the presence of beam ions. The concentration of the beam ions is kept constant, $n_b = 0.08 n_e$, and the temperature T_b is varied as a parameter.

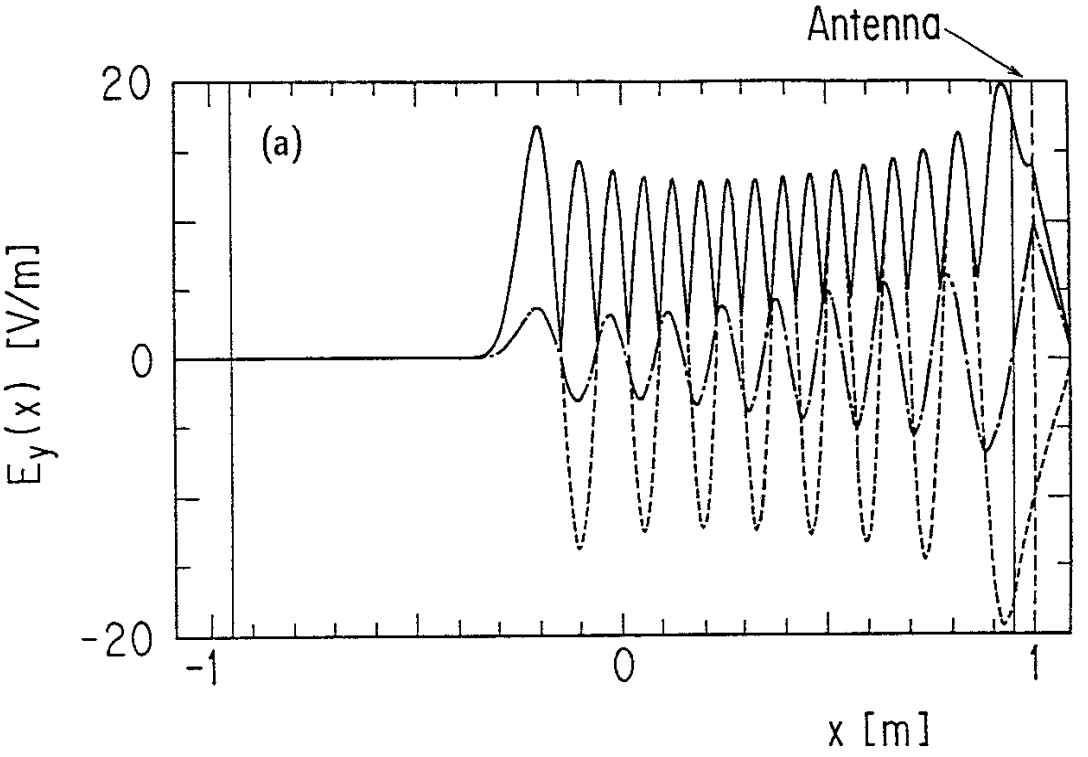

Fig. 1(a)

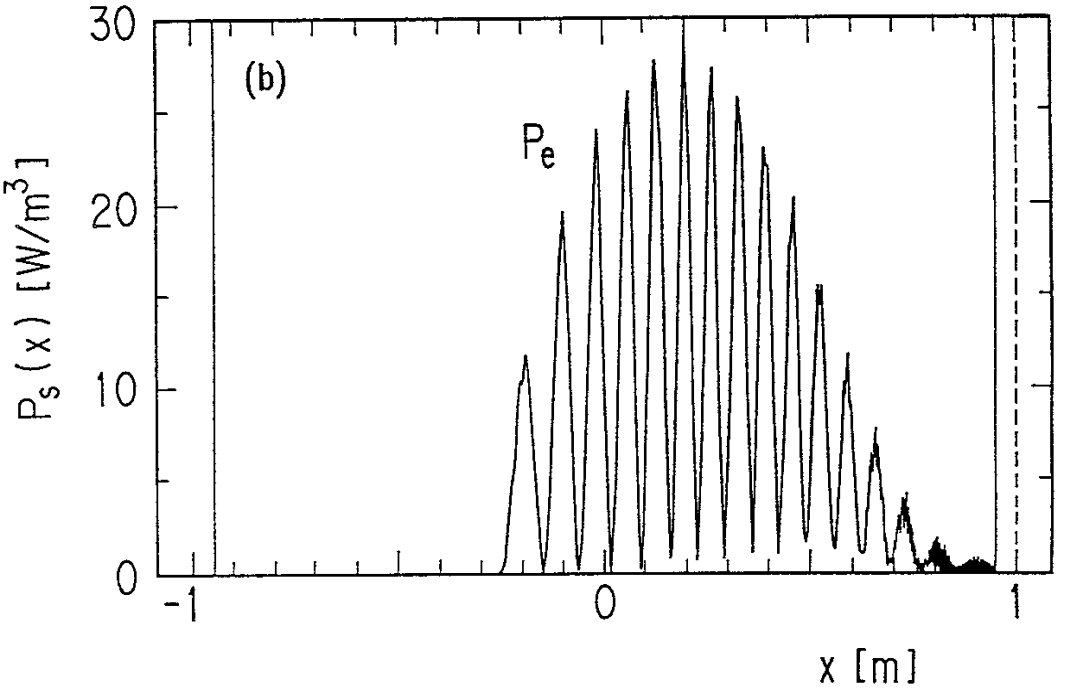

Fig. 1(b)

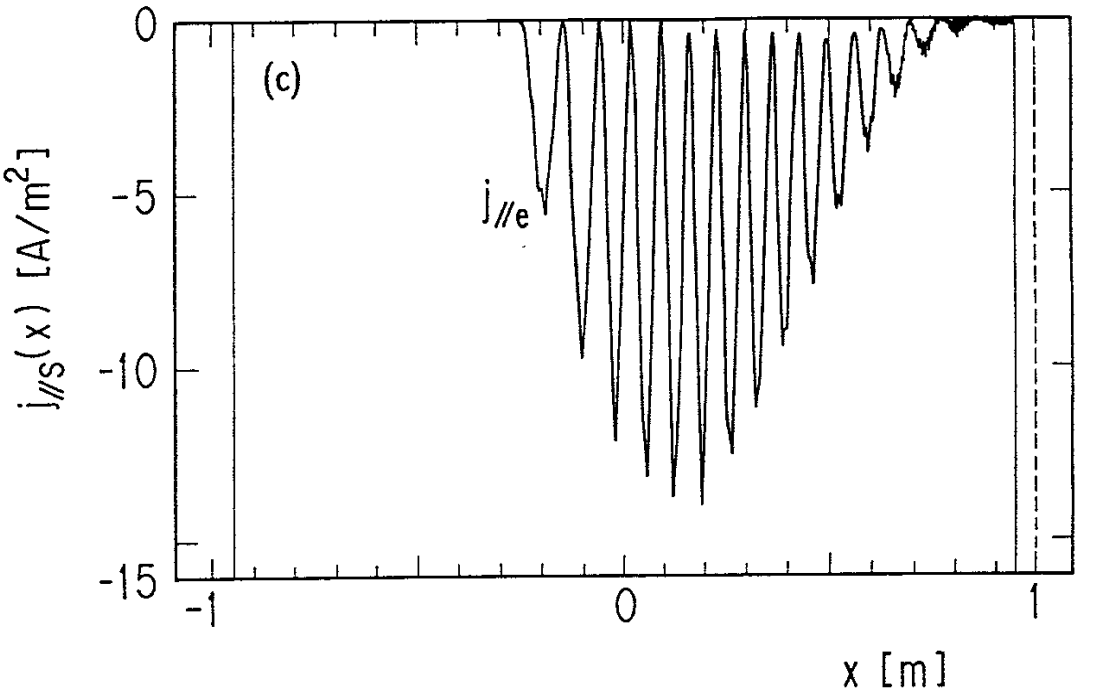

Fig. 1(c)

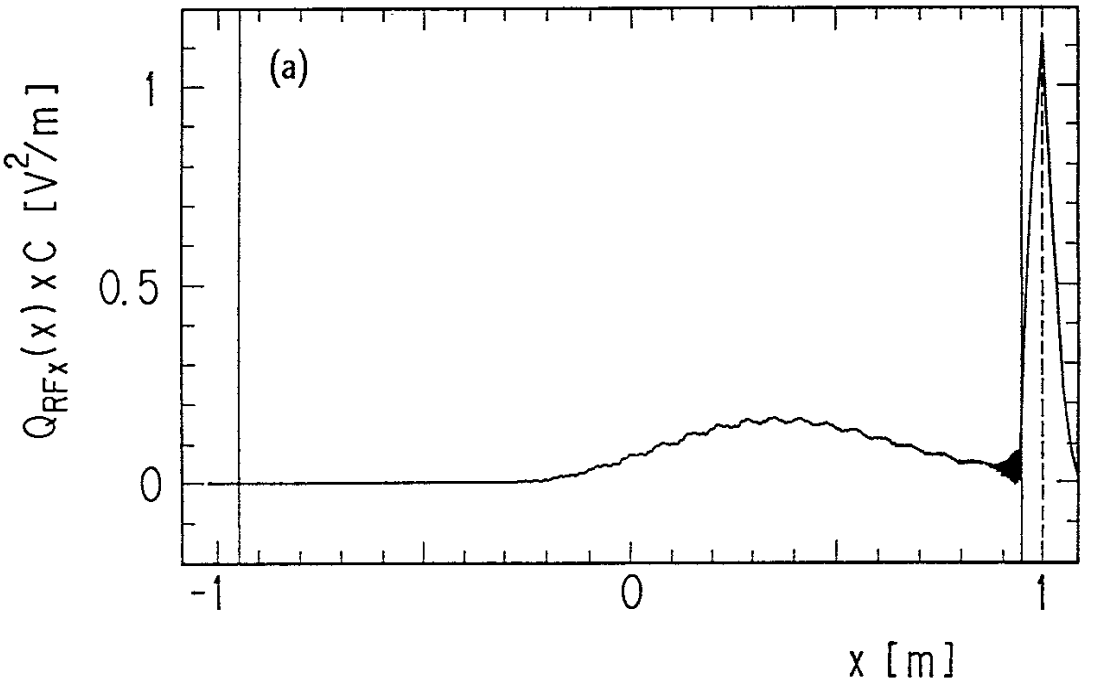

Fig. 2(a)

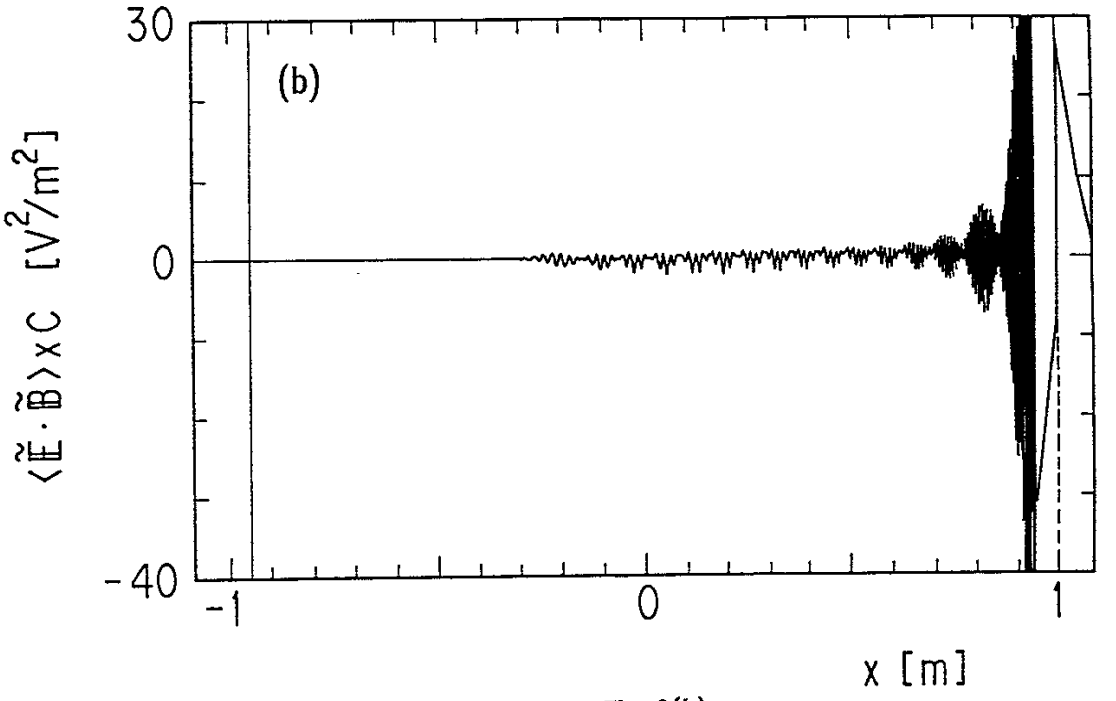
30
0
-40
(b)
$\langle \tilde{E} \cdot \tilde{B} \rangle \times C$ [V²/m²]
-1
0
1
x [m]

Fig. 2(b)

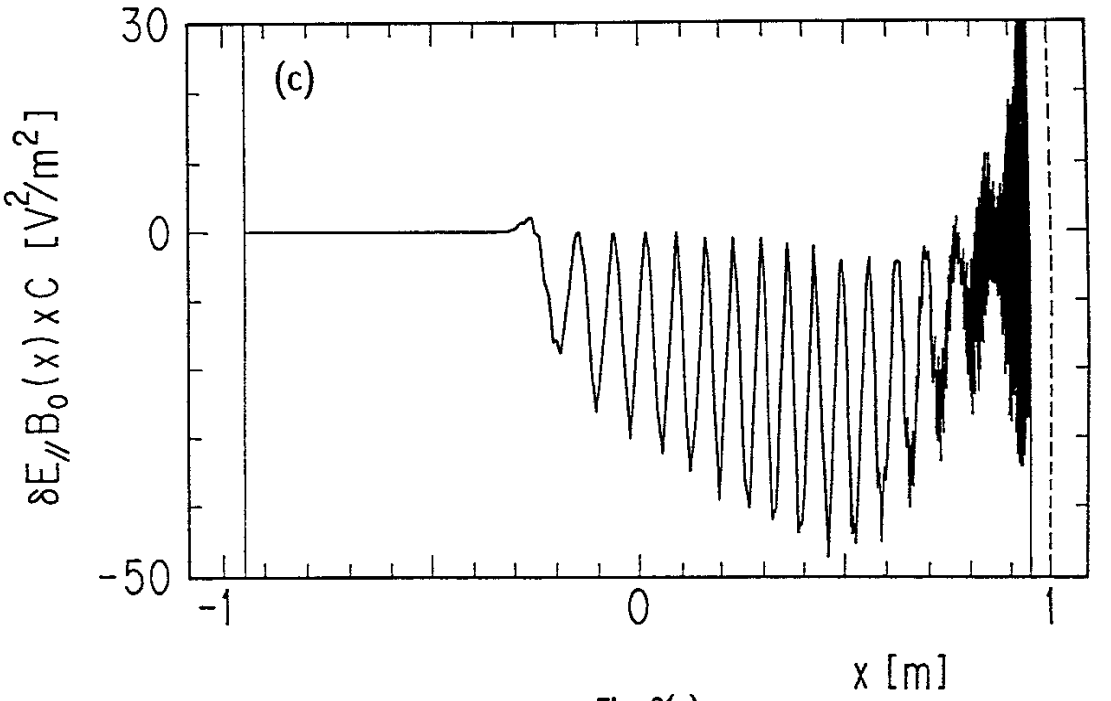
30
0
-50
(c)
$\delta E_{//} B_0(x) \times C$ [V²/m²]
-1
0
1
x [m]

Fig. 2(c)

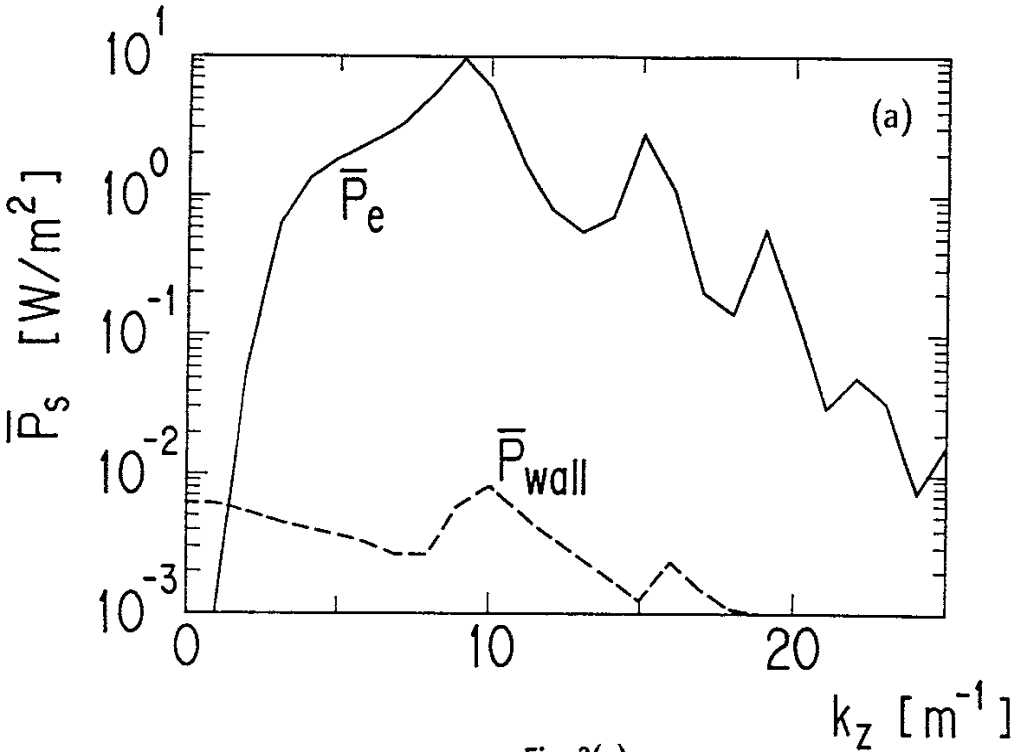
10^1
10^0
10^{-1}
10^{-2}
10^{-3}
$\bar{P}_s$ [W/m^2]
$\bar{P}_e$
$\bar{P}_{wall}$
(a)
0
10
20
k_z [m^{-1}]

Fig. 3(a)

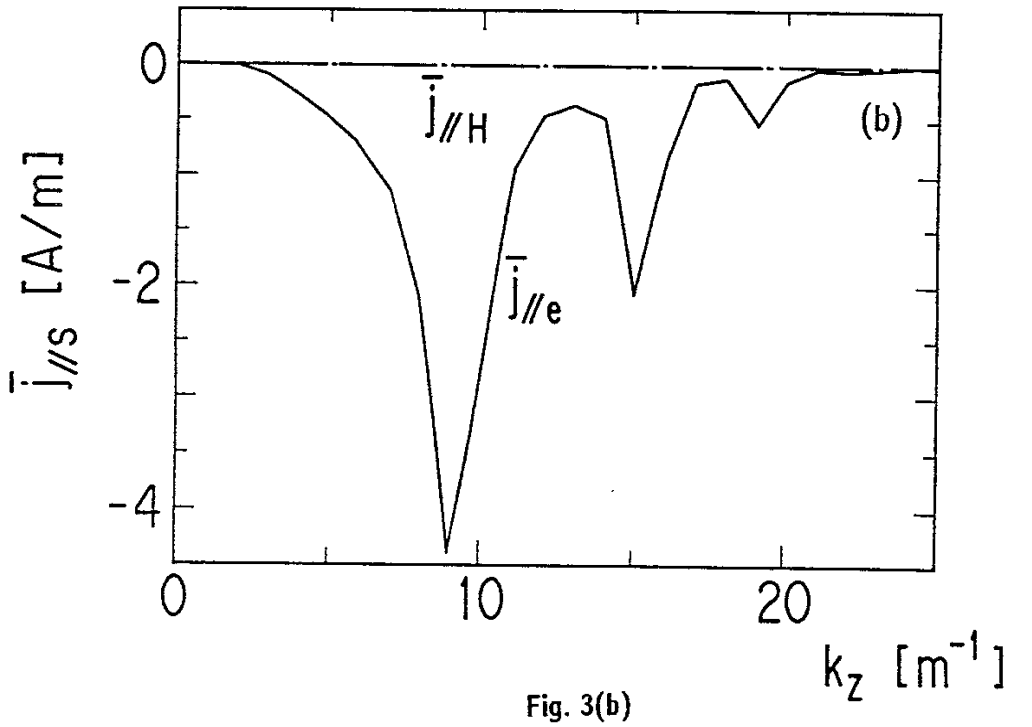
0
-2
-4
$\bar{j}_{//s}$ [A/m]
$\bar{j}_{//H}$
$\bar{j}_{//e}$
(b)
0
10
20
k_z [m^{-1}]

Fig. 3(b)

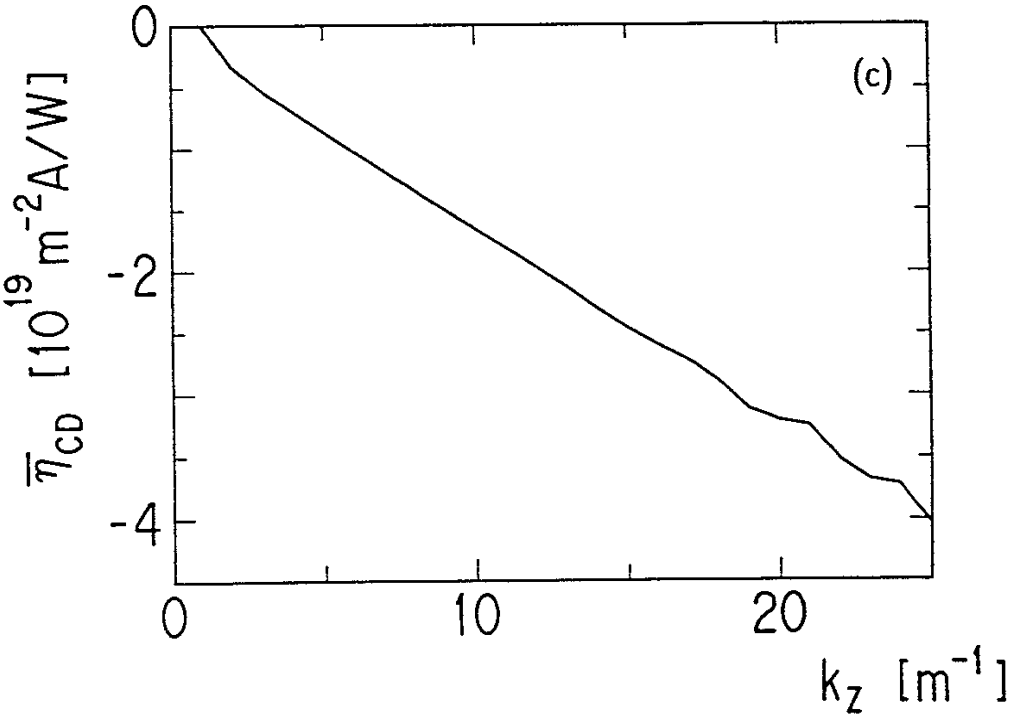
(c)
0
-2
-4
$\overline{\eta}_{CD}$ [10^{19} $m^{-2}A/W$]
0
10
20
k_z [m^{-1}]

Fig. 3(c)

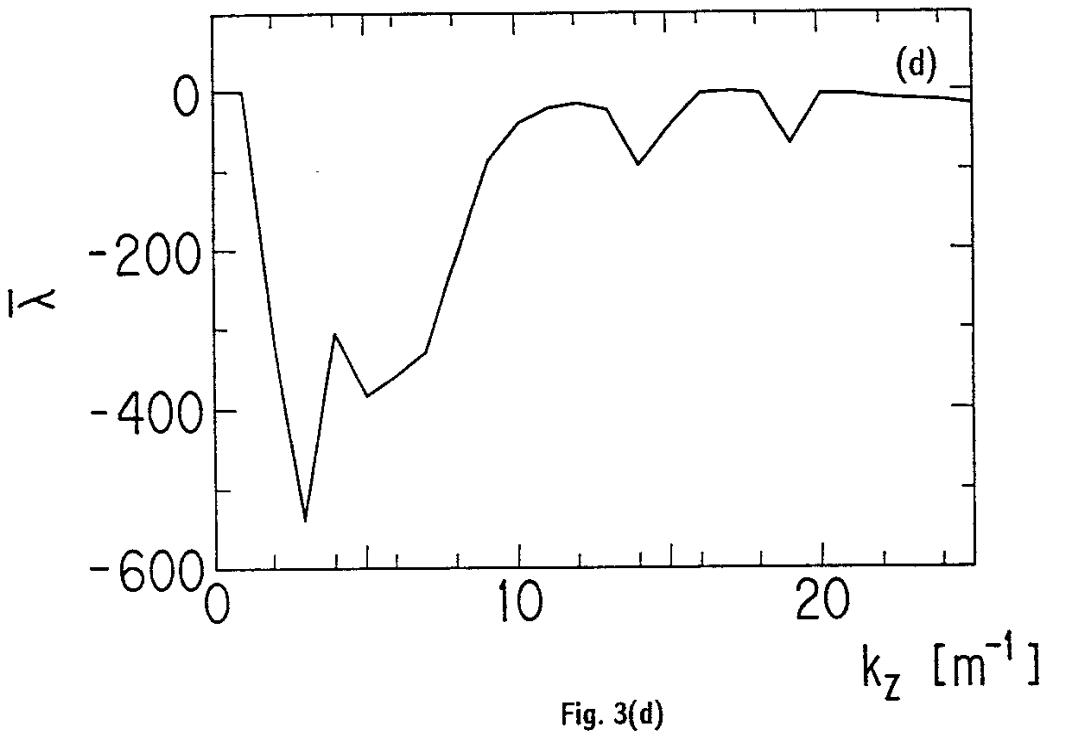
(d)
0
-200
-400
-600
$\overline{\lambda}$
0
10
20
k_z [m^{-1}]

Fig. 3(d)

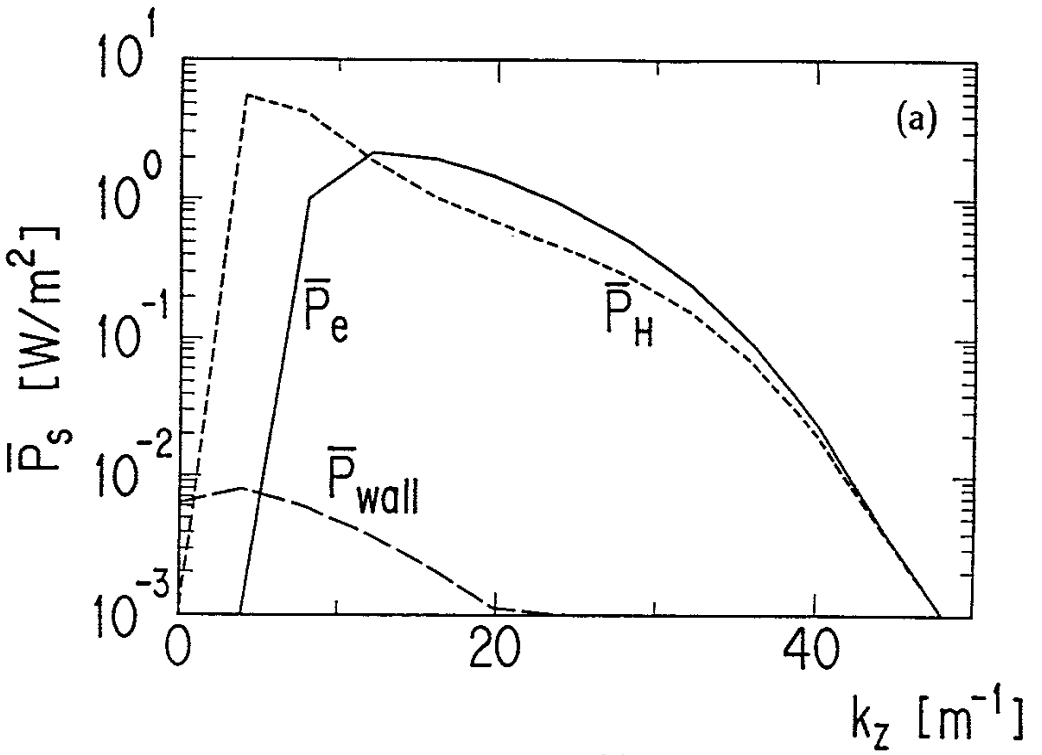
(a)
$\bar{P}_e$
$\bar{P}_H$
$\bar{P}_{wall}$
$\bar{P}_s$ [W/m^2]
10^1
10^0
10^{-1}
10^{-2}
10^{-3}
0
20
40
k_z [m^{-1}]

Fig. 4(a)

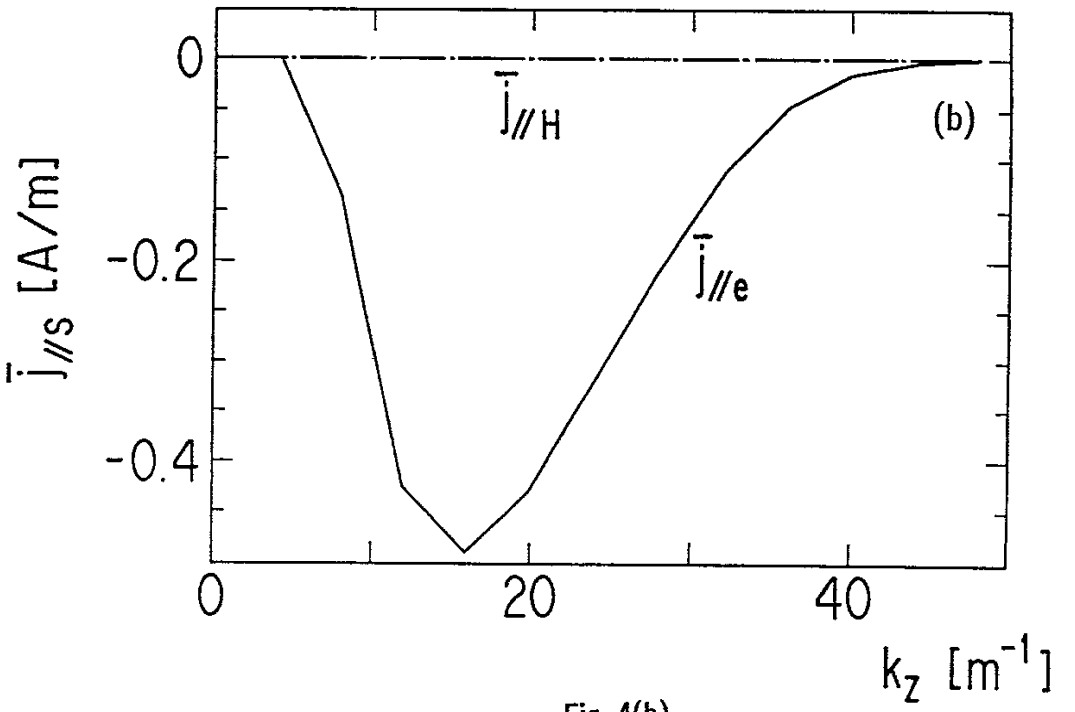
(b)
$\bar{j}_{//H}$
$\bar{j}_{//e}$
$\bar{j}_{//s}$ [A/m]
0
-0.2
-0.4
0
20
40
k_z [m^{-1}]

Fig. 4(b)

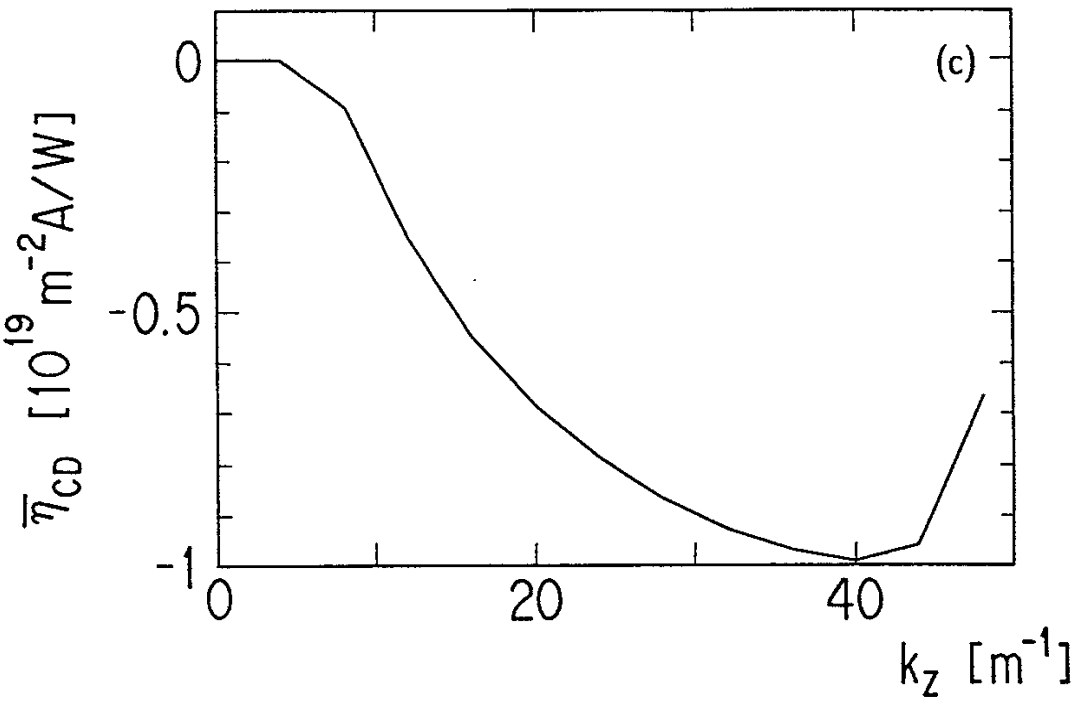
(c)
0
-0.5
-1
0
20
40
$\overline{\eta}_{CD}$ [10^{19} $m^{-2}A/W$]
k_z [m^{-1}]

Fig. 4(c)

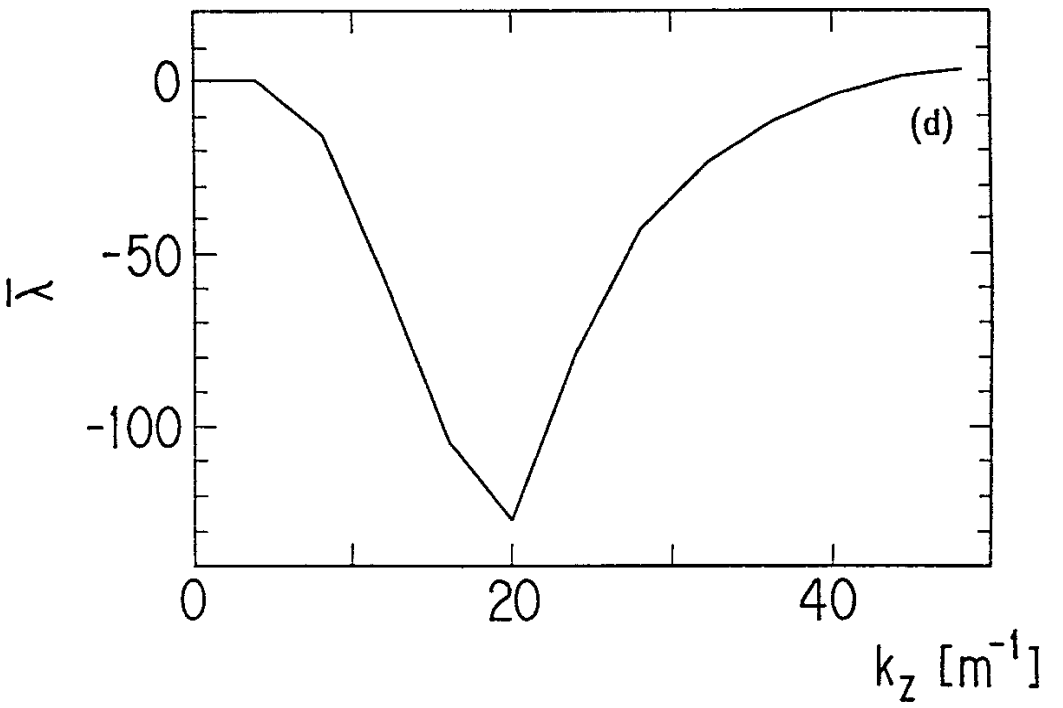
(d)
0
-50
-100
0
20
40
$\overline{\lambda}$
k_z [m^{-1}]

Fig. 4(d)

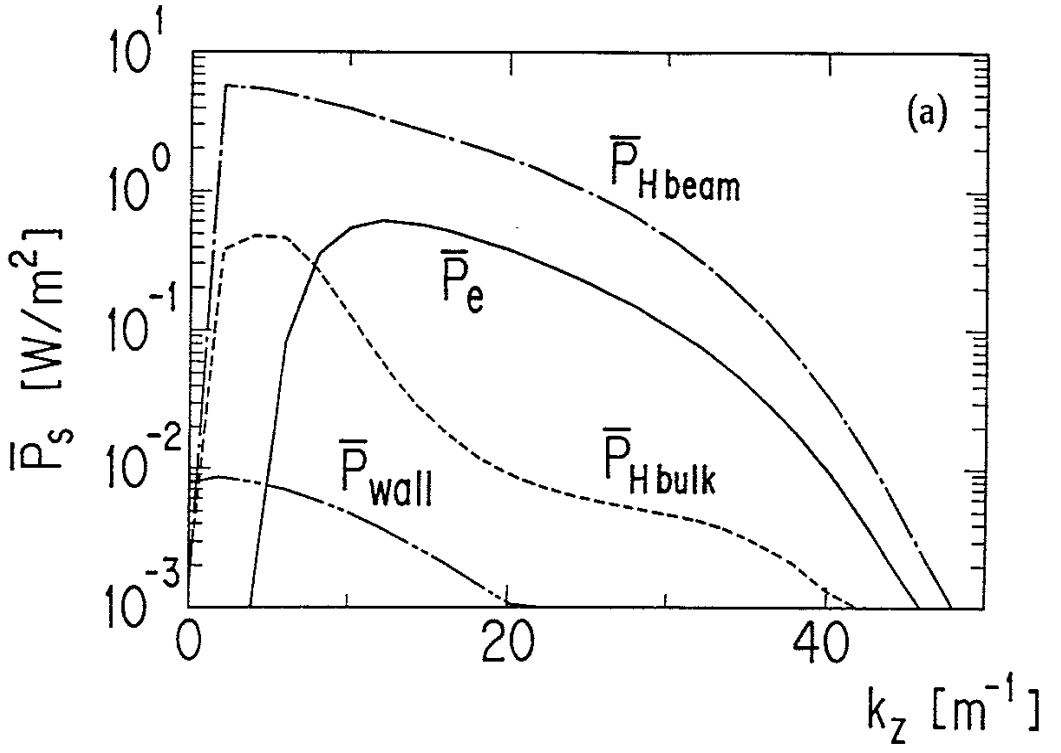
(a)
$\bar{P}_{H\,beam}$
$\bar{P}_e$
$\bar{P}_{H\,bulk}$
$\bar{P}_{wall}$
$\bar{P}_s$ [W/m^2]
10^1
10^0
10^{-1}
10^{-2}
10^{-3}
0
20
40
k_z [m^{-1}]

Fig. 5(a)

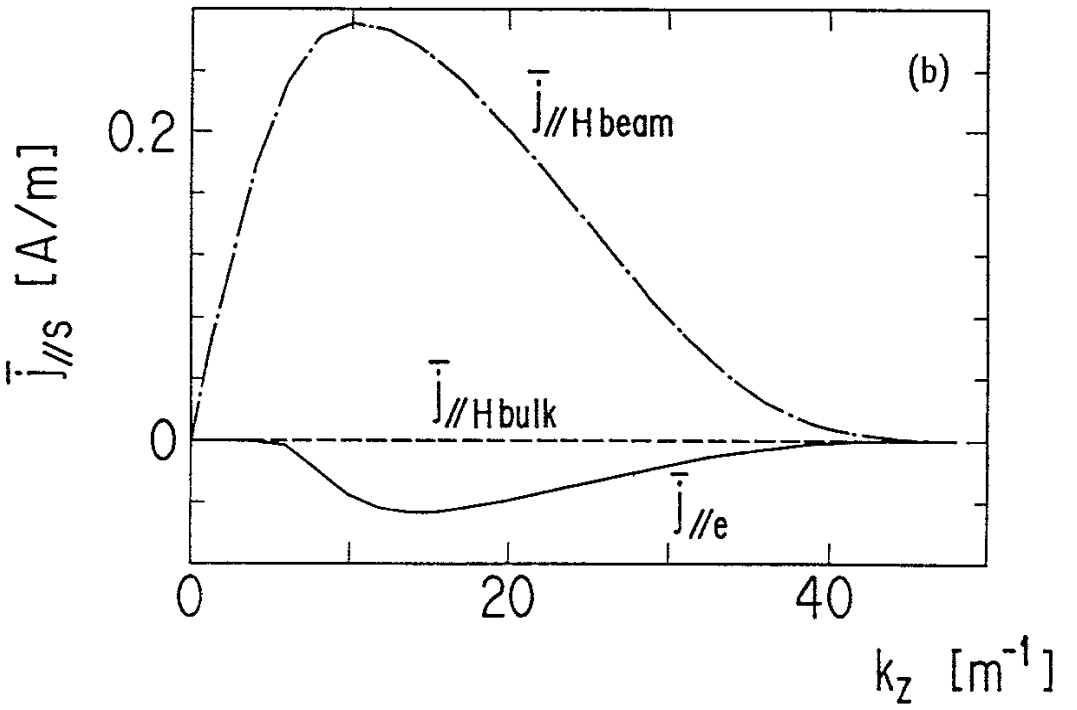
(b)
$\bar{j}_{//H\,beam}$
$\bar{j}_{//H\,bulk}$
$\bar{j}_{//e}$
$\bar{j}_{//s}$ [A/m]
0.2
0
0
20
40
k_z [m^{-1}]

Fig. 5(b)

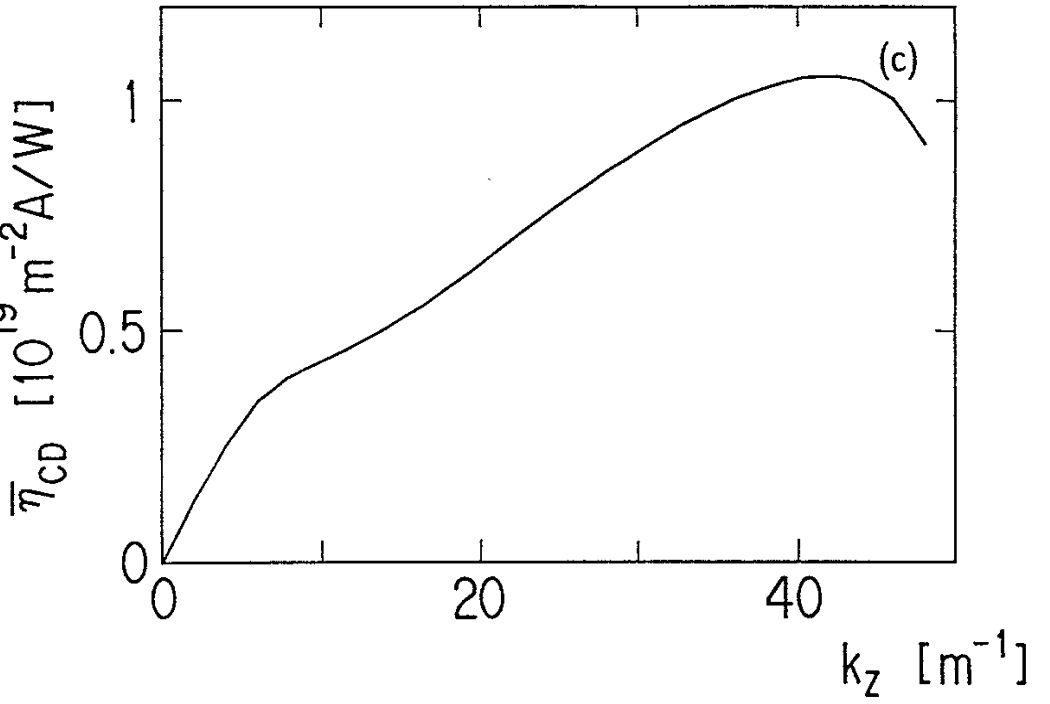
(c)
1
0.5
0
0
20
40
$\overline{\eta}_{CD}$ [10^{19} $m^{-2}A/W$]
k_z [m^{-1}]

Fig. 5(c)

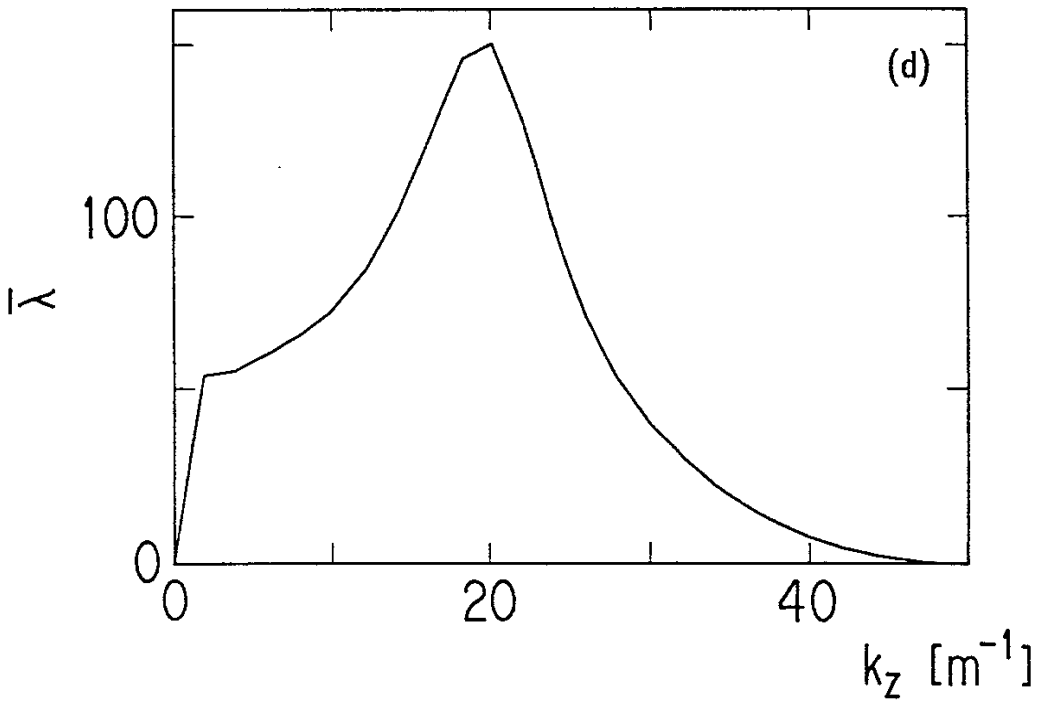
(d)
100
0
0
20
40
$\overline{\lambda}$
k_z [m^{-1}]

Fig. 5(d)

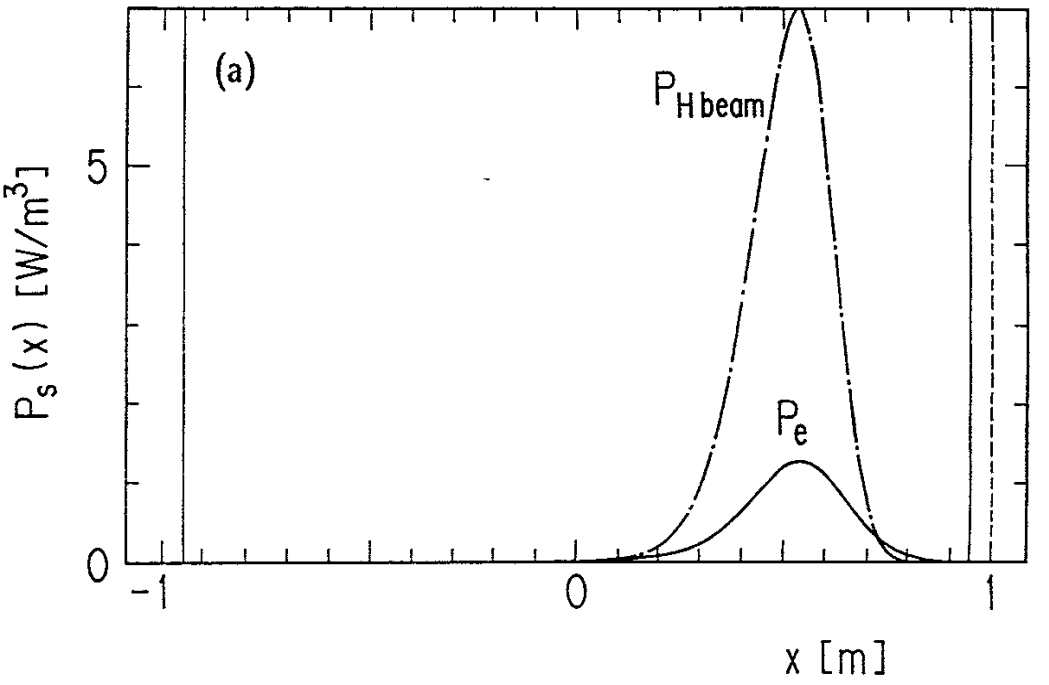
(a)
$P_{H\,beam}$
P_e
$P_s(x)$ [W/m^3]
5
0
-1
0
1
x [m]

Fig. 6(a)

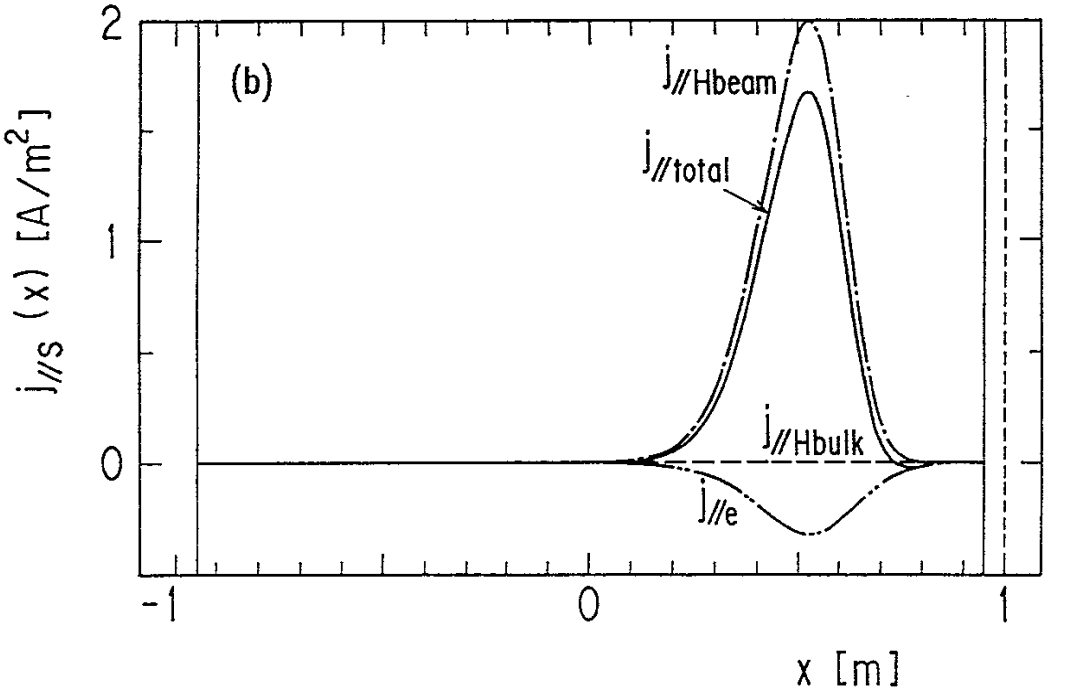
(b)
$j_{//Hbeam}$
$j_{//total}$
$j_{//Hbulk}$
$j_{//e}$
$j_{//s}(x)$ [A/m^2]
2
1
0
-1
0
1
x [m]

Fig. 6(b)

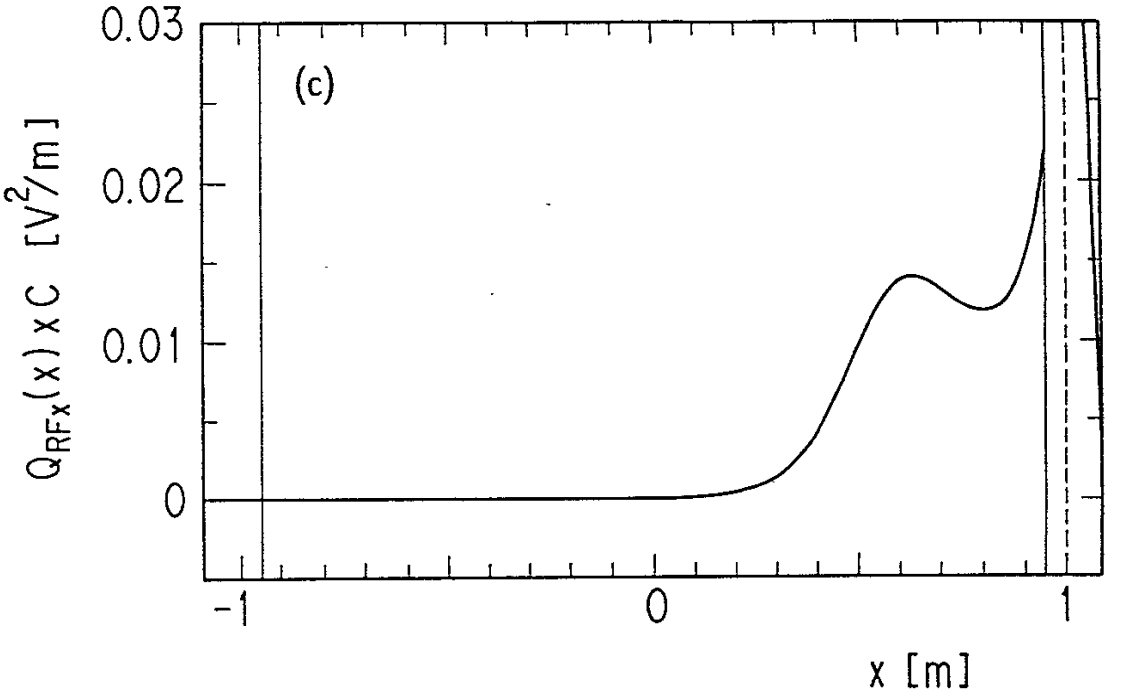
(c)
0.03
0.02
0.01
0
-1
0
1
x [m]
$Q_{RFx}(x) \times C$ [V^2/m]

Fig. 6(c)

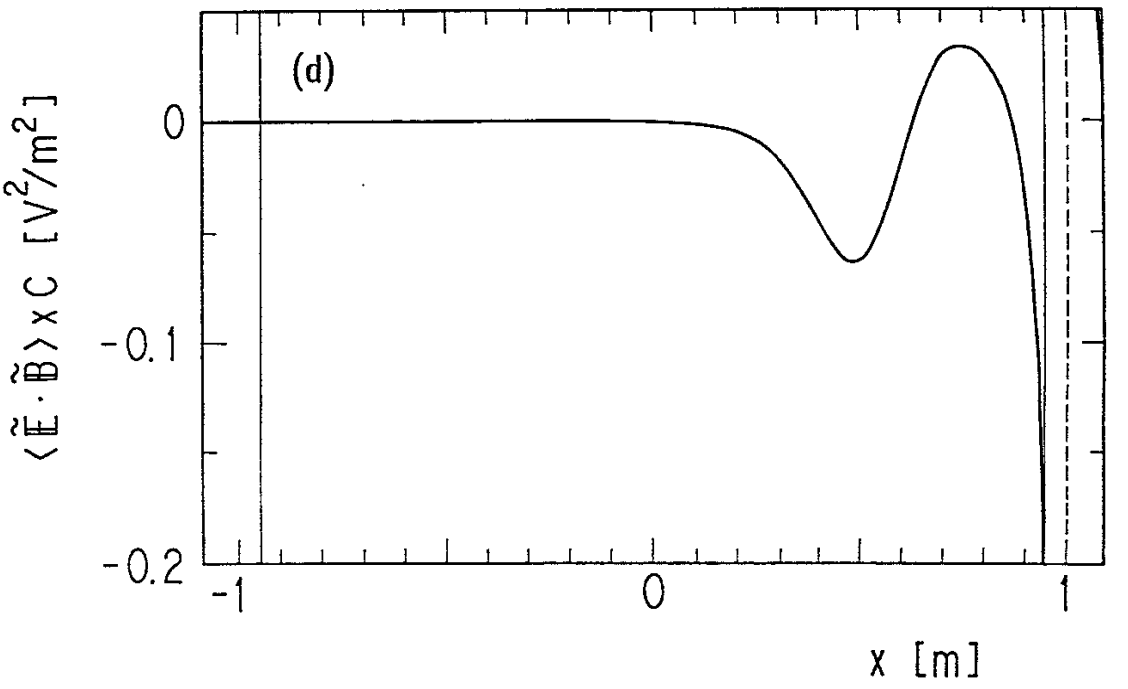
(d)
0
-0.1
-0.2
-1
0
1
x [m]
$\langle \tilde{E} \cdot \tilde{B} \rangle \times C$ [V^2/m^2]

Fig. 6(d)

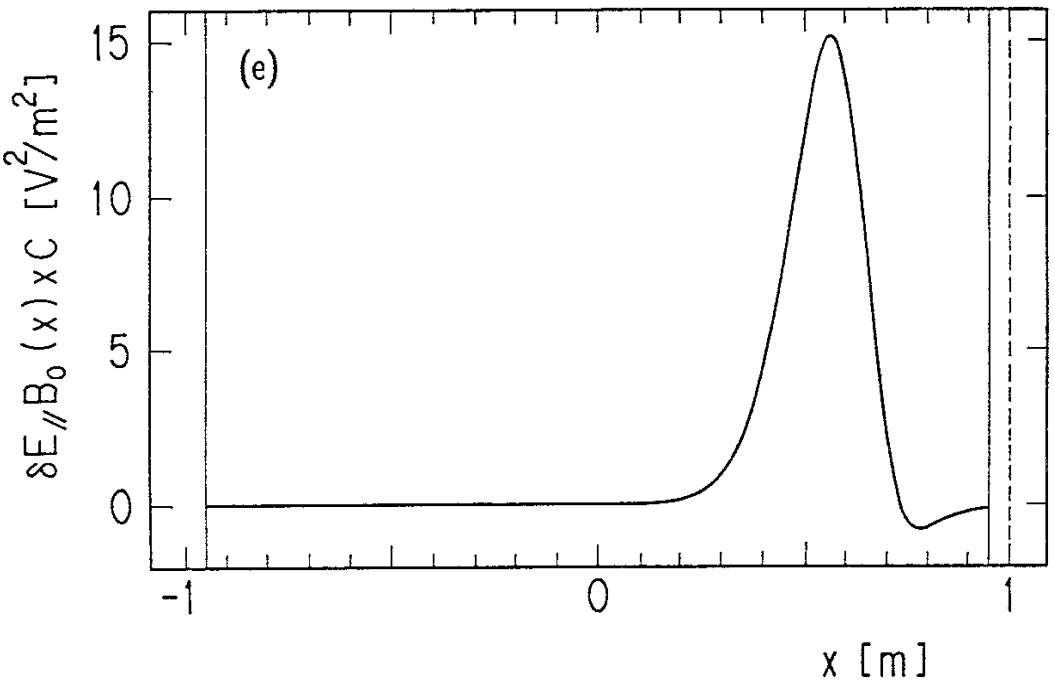
(e)
15
10
5
0
-1
0
1
x [m]
δE// B0 (x) x C [V²/m²]

Fig. 6(e)

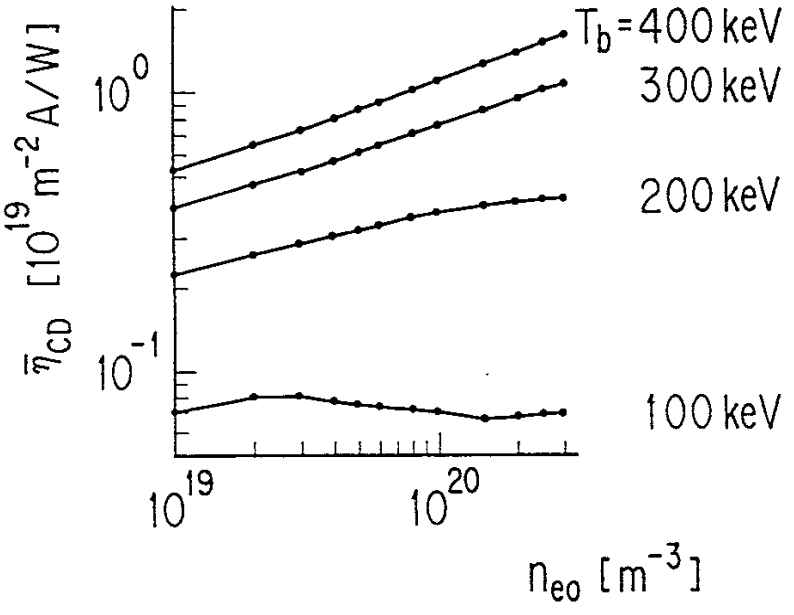
Tb = 400 keV
300 keV
200 keV
100 keV
10⁰
10⁻¹
10¹⁹
10²⁰
neo [m⁻³]
η̄CD [10¹⁹ m⁻² A/W]

Fig. 7

Publication List of NIFS Series

NIFS-1 A. Iiyoshi, M. Fujiwara, O. Motojima, J. Todoroki, N. Ohyabu and K. Yamazaki, *Design Study of the Large Helical Device* ; Jan. 1990

NIFS-2 N. Ueda, K. Itoh and S.-I. Itoh, *Numerical Studies on Divertor Plasmas in Helical Systems* ; Jan. 1990

NIFS-3 Yoshi H. Ichikawa, Y. Nomura and T. Kamimura, *Period-3 Catastrophe and Enhanced Diffusion in Two-Dimensional Hamiltonian Systems* ; Jan. 1990

NIFS-4 S.-I. Itoh and K. Itoh, *Change of Transport at L- and H-mode Transition* ; Jan. 1990

NIFS-5 Y. Nomura, S. Y. Kim, T. Kamimura and Y. H. Ichikawa, *Symmetry and Island Structure of the Standard Map* ; Feb. 1990

NIFS-6 Y. Nomura, T. Kamimura and Y. H. Ichikawa, *Stochastic Properties of the Plasma Wave Heating Map* ; Feb. 1990

NIFS-7 T. Hayashi, T. Sato and A. Takei, *Three Dimensional Studies of Helical Equilibria and Magnetic Surface Breaking Due to the Finite Beta Effect* ; Feb. 1990

NIFS-8 S.-I. Itoh, *A Model of Peaked Density Profile and Inward Pinch in Tokamaks* ; Feb. 1990

NIFS-9 H. Sanuki, J. Todoroki and T. Kamimura, *Spatial Structure of Particle-Orbit Loss Regions in $l=2$ Helical Systems* ; Feb. 1990

NIFS-10 J. Todoroki, *Adiabatic Invariant and Evaluation of Particle Loss in Helical Torus* ; Feb. 1990

NIFS-11 K. Itoh and S.-I. Itoh, *Effect of Confinement of SoL Plasma on Core Temperature Profile* ; Feb. 1990

NIFS-12 T. Kato, *Plasma Diagnostics and Atomic Processes* ; Feb. 1990

NIFS-13 K. Itoh, H. Sanuki, J. Todoroki, T. Kamimura, S.-I. Itoh, A. Fukuyama and K. Hanatani, *Loss Cone Region in Toroidal Helical Systems* ; Feb. 1990

NIFS-14 K. Urata, T. Hatori and T. Amano, *Current Bubble Formation by Nonlinear Coupling of Resistive Tearing Modes* ; Feb. 1990

NIFS-15 N. Ohyabu, *An Empirical Scaling of the Thermal Diffusivity Applicable to Both L- and H-Mode Discharges* ; Feb. 1990

NIFS-16 T. Hatori, *Magnetohydrodynamic Cellular Automata* ; Feb. 1990

NIFS-17 K. Nagasaki and K. Itoh, *Magnetic Field Structure near the Plasma Boundary in Helical Systems and Divertor Tokamaks* ; Feb. 1990

NIFS-18 J. Todoroki, *Calculation of Magnetic Field of Helical Coils* ; Feb. 1990

NIFS-19 K. Kawahata, M. Sakamoto, J. Fujita, H. Matsuo and K. Sakai, *Calibration Source for Electron Cyclotron Emission Measurements;* Feb. 1990

NIFS-20 Y. Ueda, S. Yoshida, H. B. Stewart and J. M. T. Thompson, F. R. S., *Basin Explosions and Escape Phenomena in the Twin-Well Duffing Oscillator : Compound Global Bifurcations Organizing Behaviour* ; Feb. 1990

NIFS-21 Y. Takase, T. Watari, R. Kumazawa, T. Seki, K. Adati, R. Ando, T. Aoki, Y. Hamada, S. Hirokura, K. Ida, E. Kako, K. Kawahata, Y. Kawasumi, K. Masai, K. Narihara, K. Ohkubo, M. Sakamoto, F. Shimpo, Y. Taniguchi, K. Toi and T. Tsuzuki, *Fast Wave Heating at Intermediate Ion Cyclotron Harmonics on the JIPP T-IIU Tokamak;* Feb. 1990

NIFS-22 R. Horiuchi and T. Sato, *The Meandering Orbit Effect on Stabilization of the Tilting Instability in a Field-Reversed Configuration* ; Mar. 1990

NIFS-23 K. Ida, K. Kawahata, K. Toi, T. Watari, O. Kaneko, Y. Ogawa, H. Sanuki, K. Adati, R. Akiyama, A. Ando, R. Ando, Y. Hamada, S. Hidekuma, S. Hirokura, A. Karita, T. Kawamoto, Y. Kawasumi, M. Kojima, R. Kumazawa, T. Kuroda, K. Masai, S. Morita, K. Narihara, K.Ohkubo, Y. Oka, S. Okajima, T. Ozaki, M. Sakamoto, M. Sasao, K. Sato, K. N. Sato, T. Seki, F. Shimpo, Y. Taniguchi, T. Tsuzuki and H. Yamada, *Observation of Plasma Toroidal Rotations Driven by the Electric Field Due to a Loss of Ions* ; Mar. 1990

NIFS-24 S.-I. Itoh, N. Ueda, and K. Itoh, *Simulation Study of Scalings in Scrape-Off Layer Plasma by Two Dimensional Transport Code* ; Mar. 1990

NIFS-25 B. Bhattacharyya, T. Watanabe and Kyoji Nishikawa, *Single Particle and Fluid Picture for Ponderomotive Drift in Nonuniform Plasmas;* Apr. 1990

NIFS-26 K. Ida, S. Hidekuma, Y. Miura, T. Fujita, M. Mori, K. Hoshino, N. Suzuki, T. Yamauchi and JFT-2M Group, *Edge Electric Field Profiles of H-mode Plasmas in JFT-2M Tokamak* ; Apr. 1990

NIFS-27 N. Nakajima and M. Okamoto, *Beam-Driven Currents in the 1/ v Regime in a Helical System* ; Apr. 1990

NIFS-28 K. Itoh, K. Nagasaki and S.-I. Itoh, *Heat Deposition on the Partial Limiter*; Apr. 1990

NIFS-29 S.-I. Itoh, A. Fukuyama and K. Itoh, *Fokker-Plank Equation in the Presence of Anomalous Diffusion* ; May 1990

NIFS-30 K. Yamazaki, O. Motojima, M. Asao, M. Fujiwara and A. Iiyoshi, *Design Scalings and Optimizations for Super-Conducting Large Helical Devices* ; May 1990

NIFS-31 H. Sanuki, T. Kamimura, K. Hanatani, K. Itoh and J. Todoroki, *Effects of Electric Field on Particle Drift Orbits in a $l=2$ Torsatron* ; May 1990

NIFS-32 Yoshi H. Ichikawa, *Experiments and Applications of Soliton Physics;* June 1990

NIFS-33 S.-I. Itoh, *Anomalous Viscosity due to Drift Wave Turbulence* ; June 1990

NIFS DATA-1 Y. Yamamura, T. Takiguchi and H. Tawara, *Data Compilation of Angular Distributions of Sputtered Atoms* ; Jan. 1990

NIFS DATA-2 T. Kato, J. Lang and K. E. Berrington, *Intensity Ratios of Emission Lines from OV Ions for Temperature and Density Diagnostics* ; Mar. 1990

NIFS DATA-3 T. Kaneko, *Partial Electronic Straggling Cross Sections of Atoms for Protons* ; Mar. 1990

NIFS DATA-4 T. Fujimoto, K. Sawada and K. Takahata, *Cross Section for Production of Excited Hydrogen Atoms Following Dissociative Excitation of Molecular Hydrogen by Electron Impact* ; Mar. 1990

NIFS DATA-5 H. Tawara, *Some Electron Detachment Data for H^- Ions in Collisions with Electrons, Ions, Atoms and Molecules– an Alternative Approach to High Energy Neutral Beam Production for Plasma Heating–* ; Apr. 1990

NIFS TECH-1 H. Bolt and A. Miyahara, *Runaway-Electron – Materials Interaction Studies* ; Mar. 1990

NIFS PROC-1 *U.S.-Japan Workshop on Comparison of Theoretical and Experimental Transport in Toroidal Systems Oct. 23-27, 1989* ; Mar. 1990

NIFS PROC-2 *Structures in Confined Plasmas –Proceedings of Workshop of US-Japan Joint Institute for Fusion Theory Program–* ; Mar. 1990

NIFS PROC-3 *Proceedings of the First International Toki Conference on Plasma Physics and Controlled Nuclear Fusion –Next Generation Experiments in Helical Systems– Dec. 4-7, 1989* ; Mar. 1990